

Regression-based projection for learning Mori–Zwanzig operators

Yen Ting Lin^{1,†,*}, Yifeng Tian^{1,†}, Danny Perez³, and Daniel Livescu²

¹*Information Sciences Group, Computer, Computational and Statistical Sciences Division (CCS-3), Los Alamos National Laboratory, Los Alamos, NM 87545, USA*

²*Computational Physics and Methods Group, Computer, Computational and Statistical Sciences Division (CCS-2), Los Alamos National Laboratory, Los Alamos, NM 87545, USA*

³*Physics and Chemistry of Materials Group, Theoretical Division (T-1), Los Alamos National Laboratory, Los Alamos, NM 87545, USA*

[†]*These authors contributed equally.*

^{*}*Corresponding author: yentingl@lanl.gov*

June 23, 2022

Abstract

We propose to adopt statistical regression as the projection operator to enable data-driven learning of the operators in the Mori–Zwanzig formalism. We present a principled method to extract the Markov and memory operators for any regression models. We show that the choice of linear regression results in a recently proposed data-driven learning algorithm based on Mori’s projection operator, which is a higher-order approximate Koopman learning method. We show that more expressive nonlinear regression models naturally fill in the gap between the highly idealized and computationally efficient Mori’s projection operator and the most optimal yet computationally infeasible Zwanzig’s projection operator. We performed numerical experiments and extracted the operators for an array of regression-based projections, including linear, polynomial, spline, and neural-network-based regressions, showing a progressive improvement as the complexity of the regression model increased. Our proposition provides a general framework to extract memory-dependent corrections and can be readily applied to an array of data-driven learning methods for stationary dynamical systems in the literature.

Keywords: Mori–Zwanzig formalism, Koopman representation, nonlinear projection operators, data-driven learning, regression, neural networks

AMS subject classifications: 37M19, 37M99, 46N55, 65P99, 82C31

1 Introduction

More than half a century ago, Mori [1] and Zwanzig [2] developed a mathematically rigorous formalism for constructing reduced-order models for dynamical systems in non-equilibrium

statistical mechanics. In this context, the typical degrees of the freedom of a system are of the order of Avogadro's number. In contrast to tracking the dynamics of each degree of freedom, reduced-order models (also referred to as the coarse-grained models in the context of statistical physics) are developed to describe the dynamics of a relatively small number of variables of interest. In the jargon of model coarse-graining, this set of dynamic variables is referred to as the “resolved” variables, and the rest degrees of freedom in the system is referred to as the “unresolved” ones. Reduced-order models are particularly useful in describing the emergent phenomena at the mesoscopic or macroscopic scales. They are also more computationally efficient to simulate, and thus play an essential role in bridging multiscale models.

The key difficulty in constructing reduced-order models is the *closure problem*: one must quantify the effect of the unresolved variables before self-contained evolutionary equations of the resolved variables can be prescribed. To solve the closure problem, Mori and Zwanzig adopted an elegant approach which uses functional projections. Formally, a pre-specified projection operator is used to map any function which depends on both resolved and unresolved variables to a function that only depends on the resolved variables. As the latter does not depend on the unresolved information, one can then prescribe a set of evolutionary equations for the resolved variables. The dynamical system in terms of only the projected functions is of course only an approximation of the true dynamics. The Mori–Zwanzig (MZ) formalism further quantifies the error of the approximation and derives how the error would propagate into the future by the dynamics. The central result of the Mori–Zwanzig formalism is the Generalized Langevin Equation, which stipulates that the evolutionary equations of the resolved variables do not only depend on their instantaneous values but also their past history. As a mathematically exact formula, the memory dependence, which depends critically on the choice of the resolved variables and the projection operator, quantifies the interactions between the resolved and unresolved degrees of freedom.

Theoretically speaking, there are infinitely many choices of the projection operators. In the literature, the commonly chosen projections include (1) Mori’s linear projection [1], (2) finite-rank projection operator [3], which is Mori’s projection with a set of orthonormal basis functions, (3) projection by assigning unresolved variables to zero [4, 5], and (4) Zwanzig’s fully nonlinear projection [2, 3]. It is generally difficult to derive analytic expressions for the Mori–Zwanzig formalism. Several recent studies [6, 7, 8, 9, 10, 11, 12] have established that with Mori’s linear projection operator, it is possible to adopt a data-driven approach to learn the Mori–Zwanzig operators using the time series of the resolved dynamics. In addition, it was shown [11] that these methods provide higher-order and memory-dependent corrections to existing data-driven learning of the approximate Koopman operators [13, 14, 15, 16].

In spite of being a consistent theoretical framework to the approximate Koopman learning, Mori’s projection operator is greatly limited by its linear nature. That is, after the projection, all functions must be expressed as linear combinations of a set of *a priori* specified resolved variables. The quality of the prediction thus solely depends on the choice of the resolved variables. To the authors’ best knowledge, there is no principled way to select an optimal set of resolved variables for general dynamical systems. With a non-optimal choice, the difference between the projected dynamics and the true dynamics can be unsatisfactorily large [11]. The same problem also manifests itself in the approximate Koopman learning framework [16]. Furthermore, Mori’s projection operator is not compatible with

many nonlinear closure schemes [17, 18]. Neither can we generalize the Mori’s restrictive linear projection operator to those data-driven learning methods based on modern machine learning (ML) [19, 20, 21, 22, 23], with which one relies on the neural networks (NNs) to identify the nonlinear relationship between the input (what we know at the present) and the output (what we want to predict in the future).

At the other end of the spectrum is the Zwanzig’s fully nonlinear projection operator [2, 3] which uses conditional expectation as a projection operator. Although the conditional expectation is the optimal choice of the projection operator [3], in practice, it is challenging to estimate the conditional expectations with a finite set of data, especially for high-dimensional systems that are not fully-resolved.

To address the aforementioned difficulties, we propose to adopt a regression approach to projection operators in order to bridge the gap between the linear Mori’s projection operator and the fully nonlinear Zwanzig projection operator. We show that when the regression is linear, the regression-based projection operator converges to our recently proposed data-driven methods for Mori’s projection operator [11]. Thus, the method we propose here is a superset of our previously published algorithms [11]. In addition, the regression-based projection has the capability to incorporate flexible nonlinear functions that are adaptable to the data. As such, our proposed formulation is most natural mathematical formulation for ML-based methods.

We also present numerical evidence of the approach using various nonlinear regression models, including polynomial and ridge regression, fully-connected neural networks (FCNN), and convolutional neural networks (CNN). On the one hand, we show that the nonlinear regression-based projectors out-perform the linear Mori’s projector in all the systems we investigated. As such, the method that we propose in this paper can be considered as a better replacement of our recently proposed algorithms [11]. On the other hand, we will show that the predictions of the nonlinear regression-based analysis are improved by incorporating the memory contributions prescribed by the Mori–Zwanzig formalism. As such, our proposed method is the higher-order correction of existing ML-based data-driven learning methods [19, 20, 21, 22, 23].

2 Theoretical Results

2.1 Full dynamical systems

Following the notation in [11], we consider an autonomous and deterministic dynamical system in \mathbb{R}^D following a continuous-time evolutionary equation

$$\frac{d}{dt}\boldsymbol{\phi}(t) = \mathbf{R}(\boldsymbol{\phi}(t)), \quad (1)$$

where $\boldsymbol{\phi}$ is the state in the phase space \mathbb{R}^D and $\mathbf{R} : \mathbb{R}^D \rightarrow \mathbb{R}^D$ is the flow of the system. We will assume that the flow \mathbf{R} is locally Lipschitz throughout the state space \mathbb{R}^D , so a unique $\boldsymbol{\phi}(t) \forall t \geq 0$ is guaranteed. We will denote the solution of (1) with the initial condition $\boldsymbol{\phi}_0 \in \mathbb{R}^D$ by $\boldsymbol{\phi}(t; \boldsymbol{\phi}_0)$. We will use the standard notation and denote scalars by symbols in the normal font, and vectors by symbols in bold.

2.2 Observables

In reduced-order modeling, we aim to prescribe the evolutionary equations for $M < D$ real-valued functions of the state variable ϕ , $g_i : \mathbb{R}^D \rightarrow \mathbb{R}$, $i = 1 \dots M$. We exclusively consider real-valued functions, but the theory can be straightforwardly generalized to complex-valued functions. We refer to these functions as the observables. In other context, such as material science or statistical mechanics, observables can also be referred to as descriptors, coarse-grained variables, or dynamic variables. We refer to an ‘‘observation’’ at time t as applying the set of observables to the system’s state $\phi(t; \phi_0)$, that is, a real-valued array $\{g_i(\phi(t; \phi_0))\}_{i=1}^M$. We remark that one can define an observable π_i to extract the i th component of the state ϕ at time t (that is, $\pi_i(\phi(t; \phi_0)) = \phi_i(t; \phi_0)$ [24]). In general, observables g must be measurable functions of the full state ϕ against some distribution; see below section 2.5. We will use \mathbf{g} (resp. $\mathbf{g}(\phi)$) to denote a vectorized observable $[g_1, g_2, \dots, g_M]^T$ (resp. observations, $[g_1(\phi), g_2(\phi), \dots, g_M(\phi)]^T$).

2.3 Discrete-time snapshot data

Throughout this study, we assume that the full system has been simulated and observed at discrete times, and the observations form a data set for learning the Mori–Zwanzig operators. Specifically, we rely on samples drawn from a chosen initial distribution μ (see below section 2.5) to collect the statistics of the unresolved information. The full system is prepared at $N \gg 1$ independently and identically sampled $\phi_0^{[i]} \sim \mu$, $i = 1 \dots N$. The system is then simulated and the values of the observations are registered at uniformly distributed discrete times $k\Delta$, $k = 0 \dots K - 1$. We refer to these observations as the *snapshots*. Without loss of generality, we assume $\Delta = 1$ by choosing an appropriate unit of time, unless it is specified otherwise. The full discrete-time observations thus form an $N \times M \times K$ data matrix \mathbf{D} whose (i, j, k) -entry is $g_j(\phi(k - 1; \phi_0^{[i]}))$. For ergodic systems, it is desirable to bypass sampling from a pre-specified initial distribution and use the long-time statistics instead. In this case, we generate a single but long trajectory from a randomly selected initial condition ϕ_0^r . After the initial transient time t_c , we make $K + N$ observations for every $\Delta = 1$. We use these $K + N$ observations to inform the statistics of the ergodic measure. The data matrix \mathbf{D} in this case is defined as an $N \times M \times K$ matrix whose (i, j, k) -entry is $g_j(\phi(t_c + i + k - 1; \phi_0^r))$.

2.4 Discrete-time dynamical systems

To match to the discrete-time snapshot data, we re-write the evolutionary equation (1) into a discrete-time form:

$$\phi(t + 1) = \mathbf{F}(\phi(t)), \quad (2)$$

where $\mathbf{F} : \mathbb{R}^D \rightarrow \mathbb{R}^D$ is the flow map. Locally Lipschitz condition ensures that such a mapping exists and is unique for any finite time $t \in \mathbb{Z}_{\geq 0}$. Our formulation is readily applicable to those generically discrete-time dynamical systems, in which we begin with the discrete-time formulation Eq. (2) instead of Eq. (1).

2.5 A chosen distribution and measurable functions

We assume that the number of samples N is sufficiently large to capture the statistics of the time-dependent distribution induced by the deterministic dynamics from the initial distribution μ , i.e., the solution of the generalized Liouville equation [25] corresponding to Eq. (1) :

$$\frac{\partial}{\partial t} \rho(\boldsymbol{\phi}, t) = - \sum_{i=1}^N \frac{\partial}{\partial \phi_i} [\mathbf{R}_i(\boldsymbol{\phi}) \rho(\boldsymbol{\phi}, t)], \text{ with the initial data } \rho(\boldsymbol{\phi}, 0) = \mu(\boldsymbol{\phi}), \quad (3)$$

where $\mu(\boldsymbol{\phi})$ is the probability density function of the measure μ , assuming the measure μ is dominated by the Lebesgue measure in the state space \mathbb{R}^D so $\mu(d\boldsymbol{\phi}) = \mu(\boldsymbol{\phi}) d\boldsymbol{\phi}$. When using the single trajectory to sample the ergodic distribution, we assume that N is sufficiently large such that the collected $N + K$ samples faithfully capture the statistics of the ergodic measure, i.e., the stationary solution ρ_* of Eq. (3) satisfying

$$0 = \sum_{i=1}^N \frac{\partial}{\partial \phi_i} [\mathbf{R}_i(\boldsymbol{\phi}) \rho_*(\boldsymbol{\phi})]. \quad (4)$$

In both cases, we assume that each of the observables, g_i , is an L^2 -measurable function against the induced measure. That is, if one chooses to learn from a time-dependent distribution (Eq. (3)), $\int_{\mathbb{R}^D} \rho(\boldsymbol{\phi}, t) g_i^2(\boldsymbol{\phi}) d\boldsymbol{\phi} < \infty$ for $0 \leq t \leq (K - 1) \Delta$, or if one chooses to learn from a stationary distribution (Eq. (4)), $\int_{\mathbb{R}^D} \rho_*(\boldsymbol{\phi}) |g_i(\boldsymbol{\phi})| d\boldsymbol{\phi} < \infty$.

2.6 The projection operator

Suppose all the M resolved observables are independent, we shall need another $D - M$ independent unresolved observables to uniquely specify the system's state. Denote these unresolved observables, which are also real-valued functions of the system's state $\boldsymbol{\phi}$, by $u_j : \mathbf{R}^D \rightarrow \mathbb{R}$, $j = 1 \dots D - M$. Importantly, observations of these unresolved variables, $u_j(\boldsymbol{\phi})$, are not accessible. Consider a real-valued function of the full state expressed in both the resolved and unresolved observations, $h(\{g_i(\boldsymbol{\phi})\}_{i=1}^M, \{u_j(\boldsymbol{\phi})\}_{j=1}^{D-M})$. A projection operator \mathcal{P} is an operator mapping h to another real-valued function $(\mathcal{P}h) : \mathbb{R}^D \rightarrow \mathbb{R}$ which only depends on the resolved observations. Mori-Zwanzig formalism utilizes this projection operator and decomposes any function $h(\{g_i(\boldsymbol{\phi})\}_{i=1}^M, \{u_j(\boldsymbol{\phi})\}_{j=1}^{D-M})$ into $(\mathcal{P}h)(\{g_i(\boldsymbol{\phi})\}_{i=1}^M) + h_{\perp}(\{g_i(\boldsymbol{\phi})\}_{i=1}^M, \{u_j(\boldsymbol{\phi})\}_{j=1}^{D-M})$, where $h_{\perp} := h - \mathcal{P}h$. Note that the domain of $(\mathcal{P}h)$ is still both the resolved and unresolved observations, except that the function does not explicitly depend on the unresolved $u_j(\boldsymbol{\phi})$. A projection operator \mathcal{P} must satisfy the property $\mathcal{P}^2 = \mathcal{P}$, so that for any h , $\mathcal{P}^n h = \mathcal{P}h$, $n \in \mathbb{N}$. Such a property is critical in the derivation of the MZ formalism [26].

2.7 Discrete-time Mori–Zwanzig formalism

Following the derivations in [27, 24, 11, 12], the discrete-time Mori–Zwanzig formalism prescribes the exact evolutionary equations of the observations, that for any initial condition $\phi_0 \in \mathbb{R}^D$:

$$\mathbf{g}_{n+1}(\phi_0) = \Omega^{(0)}(\mathbf{g}_n(\phi_0)) + \sum_{\ell=1}^n \Omega^{(\ell)}(\mathbf{g}_{n-\ell}(\phi_0)) + \mathbf{W}_n(\phi_0). \quad (5)$$

Here, $\mathbf{g}_n : \mathbb{R}^D \rightarrow \mathbb{R}^M$ is an $M \times 1$ vector function of the initial state ϕ_0 such that

$$\mathbf{g}_n(\phi_0) \triangleq \mathbf{g}(\phi(n; \phi_0)) \equiv \mathbf{g}(\mathbf{F}^n(\phi_0)), \quad (6)$$

noting that $\mathbf{g}_0 \equiv \mathbf{g}$. In other words, denote the finite-time (Δ) Koopman operator [28] by \mathcal{K} , $\mathbf{g}_n := \mathcal{K}^n \mathbf{g}$. For clarity, we write each component of this vector function as $\mathbf{g}_{n,i} := \mathcal{K}^n g_i$ if needed. Note that $\mathbf{g}_{0,i} = g_i$. Equation (5), referred to as the *Generalized Langevin Equation* (GLE), is the central result of the Mori–Zwanzig formalism. It states that the vectorized observation at time $n + 1$, $\mathbf{g}(\phi(n + 1; \phi_0))$, can be decomposed into three parts: (1) a Markovian function $\Omega^{(0)} : \mathbb{R}^M \rightarrow \mathbb{R}^M$ mapping the observations at time n to an $M \times 1$ vector, (2) a series of functions $\Omega^{(\ell)} : \mathbb{R}^M \rightarrow \mathbb{R}^M$, $\ell = 1, 2, \dots$, mapping past observations with a lag ℓ to $M \times 1$ vectors, and (3) the *orthogonal dynamics* that consist of observables $\mathbf{W}_n : \mathbb{R}^D \rightarrow \mathbb{R}^M$, $n = 0, 1, \dots$, mapping any initial state ϕ_0 to an $M \times 1$ vector. Interested reader can find a detailed discussion and physical interpretation of the GLE (5) in [11].

Because the GLE (5) holds true for every initial condition ϕ_0 , we can drop the function evaluation at ϕ_0 part and write succinctly an equation for the observables

$$\mathbf{g}_{n+1} = \sum_{\ell=0}^n \Omega^{(\ell)} \mathbf{g}_{n-\ell} + \mathbf{W}_n. \quad (7)$$

In writing so, we formally “lift” functions $\Omega^{(\ell)}$ in Eq. (5) to operators. That is, in Eq. (7), $\Omega^{(\ell)}$ are functional operators mapping an $M \times 1$ vector function, each of whose component is an $L^2(\mathbb{R}^D, \mu)$ -function, to another $M \times 1$ vector function, each of whose component is an $L^2(\mathbb{R}^D, \mu)$ -function again. We thus refer to $\Omega^{(\ell)}$ as the “MZ operators”. We will adopt the slightly abused notation that the same symbol $\Omega^{(\ell)}$ is used to denote both the functions in equations of observations (such as Eq. (5)) and operators in equations of observables (such as Eq. (7)).

The operators $\Omega^{(\ell)}$ and observables \mathbf{W}_n depend on the choice of the projection operator \mathcal{P} , the choice of the vectorized observable \mathbf{g} , and the finite-time (Δ) Koopman operator \mathcal{K} [27, 24]:

$$\Omega^{(n)} := \mathcal{P} \mathcal{K} [(1 - \mathcal{P}) \mathcal{K}]^n, \quad (8)$$

$$\mathbf{W}_n := [(1 - \mathcal{P}) \mathcal{K}]^{n+1} \mathbf{g}, \quad (9)$$

with $n \in \mathbb{Z}_{\geq 0}$. Because $\mathcal{P} \mathbf{W}_n = 0$ (from the fact $\mathcal{P}^2 = \mathcal{P}$), \mathbf{W}_n is often referred to as the orthogonal dynamics. From these definitions, it is straightforward to identify the following

equation which relates the memory operators to the orthogonal dynamics

$$\boldsymbol{\Omega}^{(n)} \mathbf{g} \equiv \mathcal{PKW}_{n-1}, \forall n \in \mathbb{N}. \quad (10)$$

The meaning of the above equation is more transparent when we apply the operators to any state $\boldsymbol{\phi}_0 \in \mathbb{R}^D$:

$$\boldsymbol{\Omega}^{(n)} (\mathbf{g}(\boldsymbol{\phi}_0)) \equiv \mathcal{PKW}_{n-1}(\boldsymbol{\phi}_0) \equiv \mathcal{P}((\mathbf{W}_{n-1} \circ \mathbf{F})(\boldsymbol{\phi}_0)), \forall n \in \mathbb{N}, \quad (11)$$

in which we applied the definition of the Koopman operator \mathcal{K} and used \circ to denote function composition. The above equation is referred to as the *generalized fluctuation-dissipation relation* (GFD). Below, we will demonstrate the GFD enables data-driven learning of the operators $\boldsymbol{\Omega}^{(\ell)}$'s.

2.8 Regression

Here, we provide a short description of the regression analysis. In regression analysis, the goal is to identify an optimal model f as a function of the independent variables \mathbf{x} for predicting the dependent variables \mathbf{y} . We first focus on a scalar variable y , which can be one of the many components of a vector \mathbf{y} . The model f is defined as a family of functions $f(\mathbf{x}; \boldsymbol{\theta})$ of the independent variables \mathbf{x} , parametrized by an array of parameters $\boldsymbol{\theta}$. The assumption of the (homoscedastic) regression model is that, in the most general form, there exists a random variable ε such that the dependent variable Y can be expressed as

$$Y(\mathbf{x}) = f(\mathbf{x}; \boldsymbol{\theta}_*) + \varepsilon. \quad (12)$$

Here, we use the standard capital notation to denote a random variable Y . Given a list of paired realizations $\{\mathbf{x}^{[i]}, y^{[i]}\}_{i=1}^N$, the best-fit parameters $\boldsymbol{\theta}_*$ minimizes the differences between the model prediction $f(\mathbf{x}; \boldsymbol{\theta})$ and the dependent variable Y . The best-fit parameter $\boldsymbol{\theta}_*$ is solved by minimizing a negative log-likelihood function that depends on the noise distribution. For example, for normally distributed ε , the negative log-likelihood function is proportional to the mean squared error (MSE), so the best-fit parameter is the minimizer

$$\boldsymbol{\theta}_* := \arg \min_{\boldsymbol{\theta}} \frac{1}{N} \sum_{i=1}^N (y^{[i]} - f(\mathbf{x}^{[i]}; \boldsymbol{\theta}))^2. \quad (13)$$

When the dependent variables are vectors, that is, \mathbf{y} is $P > 1$ dimensional, the cost function can be chosen as the sum of the MSE of M independent regression:

$$\boldsymbol{\theta}_* := \arg \min_{\boldsymbol{\theta}} \frac{1}{N} \sum_{i=1}^N \sum_{j=1}^P (y_j^{[i]} - f_j(\mathbf{x}^{[i]}; \boldsymbol{\theta}))^2. \quad (14)$$

We remark that the above equation comes with three assumptions about the noise model. First, in each component j of the P -dimensional \mathbf{y} , the noise ε_j is normally distributed. Second, the noise ε_j are independently and identically distributed in each of the dimension. Third, the noise is homoscedastic, which means that the variance does not depend on the

independent variable \mathbf{x} . We remark that the negative log-likelihood function can take a different form if one chooses a different noise model (e.g., correlated or heteroscedastic noise). Nevertheless, our results below are general. Thus, in the analysis below, we express a general cost function by

$$C\left(\boldsymbol{\theta}; \{\mathbf{x}^{[i]}, \mathbf{y}^{[i]}\}_{i=1}^N\right), \quad (15)$$

so the best-fit parameters $\boldsymbol{\theta}_*$ are obtained by solving a general optimization problem:

$$\boldsymbol{\theta}_* := \arg \min_{\boldsymbol{\theta}} C\left(\boldsymbol{\theta}; \{\mathbf{x}^{[i]}, \mathbf{y}^{[i]}\}_{i=1}^N\right). \quad (16)$$

2.9 Regression-based projection operators

Using the notations defined above, we treat the observations at $t = 0$, (i.e., each component of $\mathbf{g}(\boldsymbol{\phi}_0)$) as the independent variables, and the evaluations of any real-valued function $h : \mathbb{R}^D \rightarrow \mathbb{R}$ of the full state $\boldsymbol{\phi}(t; \boldsymbol{\phi}_0)$, potentially at a later time $t \geq 0$, as the dependent variable. The samples of the dependent and the independent variables are generated from the fully-resolved simulation, whose initial condition $\boldsymbol{\phi}_0^{[i]}$ is sampled from the distribution μ . Note that the time-dependent full state $\boldsymbol{\phi}(t; \boldsymbol{\phi}_0^{[i]})$ is neither resolved nor accessed, but $\mathbf{g}(\boldsymbol{\phi}_0^{[i]})$ and $h(\boldsymbol{\phi}(t; \boldsymbol{\phi}_0^{[i]}))$ are measured and registered as we simulate the dynamics. We use the samples to regress $h(\boldsymbol{\phi}(t; \boldsymbol{\phi}_0))$ on the observed values $\mathbf{g}(\boldsymbol{\phi}_0)$ using a family of functions $f(\mathbf{g}(\boldsymbol{\phi}_0); \boldsymbol{\theta})$ by minimizing a chosen cost function:

$$\boldsymbol{\theta}_* := \arg \min_{\boldsymbol{\theta}} C\left(\boldsymbol{\theta}; \left\{\mathbf{g}(\boldsymbol{\phi}_0^{[i]}), h(\boldsymbol{\phi}(t; \boldsymbol{\phi}_0^{[i]}))\right\}_{i=1}^N\right). \quad (17)$$

The best-fit $f(\cdot; \boldsymbol{\theta}_*) : \mathbb{R}^M \rightarrow \mathbb{R}$ is now a function that depends on only the resolved initial observations $\mathbf{g}(\boldsymbol{\phi}_0)$. It is clear that another regression of $f(\mathbf{g}(\boldsymbol{\phi}_0); \boldsymbol{\theta}_*)$ on the independent variables $\mathbf{g}(\boldsymbol{\phi}_0)$ using paired samples $\left\{\mathbf{g}(\boldsymbol{\phi}_0^{[i]}), f(\mathbf{g}(\boldsymbol{\phi}_0^{[i]}) ; \boldsymbol{\theta}_*)\right\}_{i=1}^N$ would result in $f(\cdot; \boldsymbol{\theta}_*)$ again. As such, regression is a projection of h to $f(\cdot; \boldsymbol{\theta}_*)$:

$$(\mathcal{P}h)(\mathbf{g}(\boldsymbol{\phi}_0)) = f(\mathbf{g}(\boldsymbol{\phi}_0); \boldsymbol{\theta}_*). \quad (18)$$

In summary, with the choice of using regression for projection, applying \mathcal{P} to any function h of the full-system state $\boldsymbol{\phi}$ results in the best-fit parametric function $f(\cdot; \boldsymbol{\theta}_*)$ of the reduced-order observations $\mathbf{g}(\boldsymbol{\phi}_0)$. With a cost function such as Eq. (14), a straightforward generalization can be made to those vector functions $\mathbf{h} : \mathbb{R}^D \rightarrow \mathbb{R}^P$, that $(\mathcal{P}\mathbf{h})(\cdot) = \mathbf{f}(\cdot; \boldsymbol{\theta}_*)$, where \mathbf{f} is a parametric family of $\mathbb{R}^M \rightarrow \mathbb{R}^P$ functions.

2.10 Learning Mori–Zwanzig operators with regression-based projection using snapshot data

We now use the snapshot data matrix \mathbf{D} to learn the MZ operators $\boldsymbol{\Omega}^{(n)}$ and orthogonal dynamics \mathbf{W}_n , $n \in \mathbb{Z}_{\geq 0}$. Setting $n = 0$, the GLE (5) with the expression Eq. (8) states

$$\mathbf{g}_1(\boldsymbol{\phi}_0) = \mathcal{P}\mathcal{K}(\mathbf{g}(\boldsymbol{\phi}_0)) + \mathbf{W}_0(\boldsymbol{\phi}_0) = \mathcal{P}[\mathbf{g}_1(\boldsymbol{\phi}_0)] + \mathbf{W}_0(\boldsymbol{\phi}_0). \quad (19)$$

for any initial state ϕ_0 . We used the definition of the Koopman operator $\mathcal{K}(\mathbf{g}(\phi_0)) = \mathbf{g}_1(\phi_0) \equiv \mathbf{g}(\phi(1; \phi_0))$, which are the observations made at one time step ahead of the initial condition ϕ_0 . These observations can be accessed in the snapshot data matrix: they are simply $\mathbf{D}(\cdot, \cdot, 2)$. So can the $\mathbf{g}(\phi_0)$, which are $\mathbf{D}(\cdot, \cdot, 1)$. The regression-based \mathcal{P} now projects the function \mathbf{g}_1 of the full initial state to an optimal function which depends on only the resolved observations $\mathbf{g}(\phi_0)$, by regressing $\mathbf{D}(\cdot, \cdot, 2)$ on $\mathbf{D}(\cdot, \cdot, 1)$. For example, using the MSE cost function (14), we solve the following optimization problem for projection:

$$C^{(0)}(\boldsymbol{\theta}; \mathbf{D}) := \frac{1}{N} \sum_{i=1}^N \sum_{j=1}^M \left[\mathbf{D}(i, j, 2) - \mathbf{f}_j \left(\{\mathbf{D}(i, k, 1)\}_{k=1}^M; \boldsymbol{\theta} \right) \right]^2, \quad (20a)$$

$$\boldsymbol{\theta}_*^{(0)} := \arg \min_{\boldsymbol{\theta}} C^{(0)}(\boldsymbol{\theta}; \mathbf{D}), \quad (20b)$$

$$\boldsymbol{\Omega}^{(0)}(\cdot) = \mathbf{f} \left(\cdot; \boldsymbol{\theta}_*^{(0)} \right), \quad (20c)$$

where $\mathbf{f}(\cdot; \boldsymbol{\theta}) : \mathbb{R}^M \rightarrow \mathbb{R}^M$ is a family of regressional functions. Next, the orthogonal dynamics \mathbf{W}_0 is identified as the *residual* of the regression problem from Eq. (19). That is, for a sample initial condition $\phi_0^{[i]}$, the j th component of the orthogonal dynamics at time 0 is:

$$\begin{aligned} (\mathbf{W}_0)_j \left(\phi_0^{[i]} \right) &= \left[\mathbf{g}_1 \left(\phi_0^{[i]} \right) - \mathcal{P} \left(\mathbf{g}_1 \left(\phi_0^{[i]} \right) \right) \right]_j \\ &= \mathbf{D}(i, j, 2) - \mathbf{f}_j \left(\{\mathbf{D}(i, k, 1)\}_{k=1}^M; \boldsymbol{\theta}_*^{(0)} \right). \end{aligned} \quad (21)$$

We now use mathematical induction to show that we can extract $\boldsymbol{\Omega}^{(n+1)}$ and samples of \mathbf{W}_{n+1} , given $\boldsymbol{\Omega}^{(\ell)}$, $\ell = 0 \dots n$ and the snapshot data matrix \mathbf{D} . We first use GLE (7) to express \mathbf{W}_n in terms of $\boldsymbol{\Omega}^{(\ell)}$ and $\mathbf{g}_{n-\ell}$:

$$\mathbf{W}_n = \mathbf{g}_{n+1} - \sum_{\ell=0}^n \boldsymbol{\Omega}^{(\ell)} \mathbf{g}_{n-\ell} = \mathbf{g} \circ \mathbf{F}^{n+1} - \sum_{\ell=0}^n \boldsymbol{\Omega}^{(\ell)} (\mathbf{g} \circ \mathbf{F}^{n-\ell}) \quad (22)$$

Then, we use the GFD, Eq. (11) to construct $\boldsymbol{\Omega}^{(n+1)}$:

$$\begin{aligned} \boldsymbol{\Omega}^{(n+1)}(\mathbf{g}(\phi_0)) &= \mathcal{P} \left[\left(\mathbf{g} \circ \mathbf{F}^{n+1} - \sum_{\ell=0}^n \boldsymbol{\Omega}^{(\ell)} (\mathbf{g} \circ \mathbf{F}^{n-\ell}) \right) \circ \mathbf{F} \right] (\phi_0) \\ &= \mathcal{P} \left(\mathbf{g}_{n+2}(\phi_0) - \sum_{\ell=0}^n \boldsymbol{\Omega}^{(\ell)} (\mathbf{g}_{n-\ell+1}(\phi_0)) \right). \end{aligned} \quad (23)$$

We recognize that $\mathbf{g}_k(\phi_0) \equiv (\mathbf{g} \circ \mathbf{F}^k)(\phi_0) \equiv \mathbf{g}(\phi(k; \phi_0))$ are the observations made at the k th step (including the initial condition). The i th sample of the j th component of $\mathbf{g}_k(\phi_0)$ is $\mathbf{D}(i, k+1, j)$. Also, $\boldsymbol{\Omega}^{(\ell)}$ can be expressed as the best-fit parametric function in the ℓ th optimization problem, $\mathbf{f}(\cdot; \boldsymbol{\theta}_*^{(\ell)})$. Recall that the projection operator \mathcal{P} is operationally an

optimization problem, similar to Eq. (20):

$$\mathbf{y}_{i,j}^{(n+1)} := \mathbf{D}(i, j, n+3) - \sum_{\ell=0}^n \mathbf{f}_j \left(\{\mathbf{D}(i, k, n-\ell+2)\}_{k=1}^M; \boldsymbol{\theta}_*^{(\ell)} \right), \quad (24a)$$

$$C^{(n+1)}(\boldsymbol{\theta}; \mathbf{D}) := \frac{1}{N} \sum_{i=1}^N \sum_{j=1}^M \left[\mathbf{y}_{i,j}^{(n+1)} - \mathbf{f}_j \left(\{\mathbf{D}(i, k, 1)\}_{k=1}^M; \boldsymbol{\theta} \right) \right]^2, \quad (24b)$$

$$\boldsymbol{\theta}_*^{(n+1)} := \arg \min_{\boldsymbol{\theta}} C^{(n+1)}(\boldsymbol{\theta}; \mathbf{D}), \quad (24c)$$

$$\boldsymbol{\Omega}^{(n+1)} \equiv \mathbf{f} \left(\cdot; \boldsymbol{\theta}_*^{(n+1)} \right). \quad (24d)$$

Thus by induction, we can iteratively extract $\boldsymbol{\Omega}^{(n)}$, $n = 0 \dots N-2$ (in total, $N-1$ operators), using the collected snapshot data matrix \mathbf{D} . Note that the family of regressional functions \mathbf{f} is kept the same for different orders of ℓ to ensure a consistent projection operator \mathcal{P} . We remark that both the orthogonality $\mathcal{P}\mathbf{W}_n = 0$ and the GFD $\boldsymbol{\Omega}^{(n+1)}\mathbf{g} = \mathcal{P}\mathcal{K}\mathbf{W}_n$ are built in by construction.

The above procedure iteratively learns the operators $\boldsymbol{\Omega}^{(\ell)}$ in the GLE (7). The GLE is a particular form of memory-dependent dynamics, which is specific to the choices of the observables \mathbf{g} and projection operator \mathcal{P} . There are other forms of memory-dependent dynamics which do not rely on an *a priori* selected projection operator, for example, the Hankel-DMD method [29]. Numerical comparison of these methods and a detailed discussion will be provided below in Secs. 3.2 and 4.

2.11 A special case: linear regression

We now show that the special choice of linear regression results in the discrete-time algorithm we proposed in [11]. For any observation $\mathbf{g}(\phi_0)$, linear regression postulates that the parametric form of \mathbf{f} is

$$\mathbf{f}(\mathbf{g}(\phi_0); \boldsymbol{\beta}) := \boldsymbol{\beta} \cdot \mathbf{g}(\phi_0). \quad (25)$$

Generally, we include the constant function that maps any ϕ to 1 in the vectorized observable \mathbf{g} to accounts for the biased term in linear regression analysis. Here, the parameters $\boldsymbol{\theta}$ is the list of entries of the $M \times M$ matrix $\boldsymbol{\beta}$. The best fit of a linear regression is analytically tractable. Define the $N \times M$ data matrix \mathbf{X} at time $k-1$ whose entries are $\mathbf{X}_{i,j}(k-1) := \mathbf{D}(i, j, k)$. The solution of Eqs. (20) is

$$\boldsymbol{\Omega}^{(0)} = \mathbf{C}(1) \cdot \mathbf{C}^{-1}(0), \quad (26)$$

where $\mathbf{C}(k) := \mathbf{X}^T(k) \cdot \mathbf{X}(0)$ is the empirical k -lag correlation matrix of the observations. Equation (26) is precisely the extracted Markov term in [11], and the approximate Koopman operator [14, 15, 16]. As for the higher orders, Eq. (24a) can be expressed as

$$\mathbf{y}^{(n+1)} := \mathbf{X}(n+2) - \sum_{\ell=0}^n \boldsymbol{\Omega}^{(\ell)} \cdot \mathbf{X}(n-\ell+1), \quad (27)$$

leading to the solution of the minimization problem Eqs. (24b)-(24d):

$$\mathbf{\Omega}^{(n+1)} = \left[\mathbf{C}(n+2) - \sum_{\ell=0}^n \mathbf{\Omega}^{(\ell)} \cdot \mathbf{C}(n-\ell+1) \right] \cdot \mathbf{C}^{-1}(0), \quad (28)$$

which is exactly the formula derived from the GLE with Mori's projection operator [11]. Thus, the linear regression-based projection is equivalent to Mori's and the finite-rank projection operators.

2.12 Making predictions and modeling orthogonal dynamics

Our goal is to iteratively use GLE (5) to make multistep predictions for the resolved observables, once the operators $\mathbf{\Omega}^{(\ell)}$'s are learned. For prediction, it is convenient to shift the time index and write the "present time" as $t = 0$, assuming the system initiated from ϕ_{-T} at $t = -T$ in the past ($T \in \mathbb{Z}_{\geq 0}$). We assume that the present and a finite number of past snapshots, $\mathbf{g}_{-\ell}(\phi_{-T})$, $\ell = 0, 1, \dots, H-1 \leq T$, are given. We will make predictions for the resolved variables at a future horizon $t = k \geq 1$, $\mathbf{g}_k(\phi_{-T})$. To achieve this, we first use a truncated GLE to predict \mathbf{g}_1 :

$$\mathbf{g}_1(\phi_{-T}) = \sum_{\ell=0}^{H-1} \mathbf{\Omega}^{(\ell)}(\mathbf{g}_{-\ell}(\phi_{-T})) + \mathbf{W}_T(\phi_{-T}). \quad (29)$$

This is a truncated GLE because only a finite length of the history is provided; terms $\mathbf{\Omega}^{(\ell)}(\mathbf{g}_{-\ell}(\phi_{-T}))$, $\ell = H \dots T$ are neglected. We show below with numerical evidence that this truncation is justifiable. Once $\mathbf{g}_1(\phi_{-T})$ is obtained, we accumulate the predicted $\mathbf{g}_1(\phi_{-T})$ into the series of observations, $\mathbf{g}_{-\ell}(\phi_{-T})$, $\ell = -1, 0, 1 \dots H-1$, and use this accumulated series to make prediction of $\mathbf{g}_2(\phi_{-T})$ using the truncated GLE (29) again:

$$\mathbf{g}_2(\phi_{-T}) = \sum_{\ell=0}^{H-1} \mathbf{\Omega}^{(\ell)}(\mathbf{g}_{1-\ell}(\phi_{-T})) + \mathbf{W}_{T+1}(\phi_{-T}). \quad (30)$$

The procedure continues until the desired horizon $k \geq 1$ is reached. Note that this procedure only needs the first H operators $\mathbf{\Omega}^{(\ell)}$, $\ell = 0 \dots H-1$. Clearly, the orthogonal dynamics \mathbf{W}_n , $n = T \dots T+k-1$, are needed in the procedure. Recall that the orthogonal dynamics encode the information in the unresolved space (Eq. (9)), so they cannot be obtained by data-driven approaches. We must then rely on modeling. However, modeling the orthogonal dynamics is challenging: it is equivalent to modeling all the $D - M$ unresolved degrees of freedom. In addition, the modeling is specific to the full dynamical system, the choice of the resolved observables, and the choice of the projection operator.

A best-case scenario is that the resolved observables are reasonably selected, and an expressive enough regression model is chosen. With a sufficiently long history length H , this leads to negligible orthogonal dynamics, i.e., the residuals of the regression analysis are small enough to be negligible. In the numerical experiments below, we assume this best-case scenario and proceed with a trivial zero-noise model $\mathbf{W}_n = 0$, $n \geq T$, despite that finite residuals are observed in the experiments.

We also tested the standard way of fitting the residual \mathbf{W}_n as independent and multivariate Gaussian distribution (independent between different time indices, and multivariate in the M observables). The results are qualitatively similar but more noisy, because the prediction are based on randomly generated samples of the distribution. As the results with the Gaussian noise model are similar but less “clean”, we will not present them in this article.

2.13 Nonlinear regression on linear functional basis vs. linear regression on nonlinear functional basis

We now juxtapose the nonlinear regression-based projection operator with the Mori’s projector, which is a linear Koopman representation with nonlinear functional basis [1, 16, 11]. Although Koopman representation is linear—potentially with nonlinear functional basis [16]—with the benefit that the learning is a simple convex problem, it comes with two shortcomings.

First, the prediction in the Koopman representation is always linear in the current and the past observations. The linearity excludes the possibility to nonlinearly relate two observations and thus, Koopman and equivalently Mori’s formalism is not compatible with nonlinear closure methods developed in model coarse-graining. On the contrary, the nonlinear regression-based projection operator is suitable for these nonlinear closure scheme.

To illustrate this problem, let us consider a hypothetical, one-dimensional nonlinear dynamical system whose state is $\phi \in \mathbb{R}^1$. Suppose we choose the linear and quadratic polynomial functions as the only observables, $\mathbf{g}(\phi) = [\phi^1, \phi^2]^T$, assuming that these polynomial functions do not span a Koopman invariant space. Now, suppose we have performed the data-driven learning and obtained the Mori–Zwanzig operators $\Omega^{(\ell)}$, $\forall \ell$, using the snapshot data and algorithms presented in [11]. With Mori’s projection, the MZ operators $\Omega^{(\ell)}$ are 2×2 matrices. Next, suppose we wish to use the learned operators and the truncated GLE (29) to make predictions for the observables, i.e., $\phi(t; \phi_0)$ and $\phi^2(t; \phi_0)$, provided a series of present and past snapshots $\mathbf{g}_0(\phi_{-T})$, $\mathbf{g}_{-1}(\phi_{-T})$, \dots , $\mathbf{g}_{-H+1}(\phi_{-T})$, $H \geq 1$. Clearly, each component of the predicted \mathbf{g}_1 by GLE (29) is a linear combination of the components of \mathbf{g}_n , $n = 0 \dots -H + 1$, and \mathbf{W}_T . Similarly, each component of \mathbf{g}_2 by GLE (5) is a linear combination of the components of \mathbf{g}_n , $n = 1 \dots -H + 2$, \mathbf{W}_T , and \mathbf{W}_{T+1} . Now the dependence on \mathbf{g}_1 can be suppressed and rewritten as a linear sum of the components \mathbf{g}_n , $n = 0 \dots -H + 1$ and \mathbf{W}_T . In general, any prediction \mathbf{g}_k , $k \geq 1$ is linear in the components of $\mathbf{g}_n = 0 \dots -H + 1$ and those of \mathbf{W}_m , $m = T \dots T + k - 1$. Note that a special *memory-less* case of $H = 1$ converges to the prediction based on the approximate Koopman methods. In any case, the predictions are always *linear combinations of the given observables*. This is inconsistent with nonlinear closure schemes, where the reduced-order models can have terms that are nonlinear in the observables.

A relevant pitfall of Mori’s projection operator is the above linear predictions cannot satisfy the trivial nonlinear relationship $\mathbf{g}_{n,2} = \mathbf{g}_{n,1}^2$, $\forall n \geq 0$, established from the definition of the Koopman operator, that for any initial condition ϕ_0 :

$$\begin{aligned} \mathbf{g}_{n,2}(\phi_0) &= (\mathcal{K}^n \mathbf{g}_2)(\phi_0) = \mathbf{g}_2(\phi(n; \phi_0)) = \phi^2(n; \phi_0) \\ &= [\mathbf{g}_1(\phi(n; \phi_0))]^2 = [(\mathcal{K}^n \mathbf{g}_1)(\phi_0)]^2 = (\mathcal{K}^n \mathbf{g}_1)^2(\phi_0) = \mathbf{g}_{n,1}^2(\phi_0). \end{aligned} \quad (31)$$

We remind the reader that we used $\mathbf{g}_{n,m}$ to denote the n th step prediction of the m th observable, here $\mathbf{g}_{0,m}(\phi_0) \triangleq \phi_0^m$. In general, such a relationship cannot be met. For example, for $n = 1$, the prediction $\mathbf{g}_{1,1} = \sum_{i=-H+1}^0 \alpha_i \mathbf{g}_{i,1} + \beta_1 \mathbf{g}_{i,2} + \mathbf{W}_1$ and $\mathbf{g}_{1,2} = \sum_{i=-H+1}^0 \gamma_i \mathbf{g}_{i,1} + \eta_i \mathbf{g}_{i,2} + \mathbf{W}_2$, with some linear coefficients α , β_i , γ_i , and δ_i , clearly cannot satisfy $\mathbf{g}_{1,1}^2 = \mathbf{g}_{1,2}$. The inconsistency in approximate Koopman or Mori's projection operator came from the choice that one always expresses $\mathbf{g}_{n,m}$, $n \geq 1$, in terms of linear combination of $\mathbf{g}_{0,1}$ and $\mathbf{g}_{0,2}$. In the numerical experiments below, we will show how the predictions based on the linear projection operator can be extremely unsatisfactory.

On the contrary, suppose we utilize a nonlinear polynomial regression on a scalar observable $g(\phi) \triangleq \phi$, so the observations are simply the values of the phase-space variable $\phi(t; \phi_{-T})$ at time t , with a comparable nonlinearity in the regressional functions, $f(x; \alpha, \beta) = \alpha x + \beta x^2$, where the parameters $\boldsymbol{\theta}$ of the regression model are two real-valued numbers (α, β) . Suppose we have carried out the nonlinear regression analysis and obtained the optimal $\boldsymbol{\theta}_*^{(\ell)}$, $\forall \ell \geq 0$. We next use the learned parameters to make prediction, provided a series of present and past snapshots $\phi(t; \phi_{-T})$, $t = 0, \dots -H + 1$. With the truncated GLE (29) and the nonlinear regression as the projection operator, the first-step prediction is

$$g_1 = \left(\sum_{\ell=0}^{H-1} \alpha_*^{(\ell)} g_{-\ell} + \beta_*^{(\ell)} g_{-\ell}^2 \right) + W_T, \quad (32)$$

which is identical to the prediction based on Mori's projection operator with two lowest polynomial functions as observables. However, in the second step, the truncated GLE would induce nonlinearity:

$$g_2 = \left(\sum_{\ell=0}^{H-1} \alpha_*^{(\ell)} g_{1-\ell} + \beta_*^{(\ell)} g_{1-\ell}^2 \right) + W_{T+1}. \quad (33)$$

The presence of g_1^2 in the above equation introduces nonlinearity in the past observables g_t , $t = 0 \dots -H + 1$ (see Eq. (32)). The predictive model now is a coarse-grained model with a nonlinear closure scheme, that it is a nonlinear dynamical system of the reduced-order variables (v. linear in the reduced-order variables with Mori's projection operator or with approximate Koopman analysis).

The second shortcoming of the approximate Koopman's computation is that its observables— $\mathbf{g}_{0,i}$'s—have to be specified *a priori*. There exist methods that leverage NNs for learning optimal observables for approximate Koopman learning [20, 21, 22, 23]. However, NNs are generally nonlinear functions of their parameters, so the joint learning problem (i.e., learning the functional basis and the approximate Koopman operator) loses linearity and cannot be cast as a Mori's projection operator. In addition, NNs are prone to over-fitting, so regularization techniques had to be imposed, leading to a different optimization problem from the original approximate Koopman [16] or Mori's [11] setup. Consequently, we could not generalize data-driven learning [11] with the linear projection operators [1, 3] for these NN-based data-driven learning methods. Contrarily, regression-based projection operators are not restricted by the linear constraint. Regression-based projection operators can accommodate nonlinear basis function optimization by postulating the parametric family of functions

are of the form $\mathbf{f}(\mathbf{x}; \boldsymbol{\theta}, \mathbf{K}) = \sum_{i=1}^M \mathbf{K} \cdot \mathbf{f}_i(\mathbf{x}; \boldsymbol{\theta})$, where \mathbf{f}_i 's are the adaptable observables parametrized by $\boldsymbol{\theta}$, and an unknown matrix \mathbf{K} characterizes the postulation that the dependent variables are linear combinations of the observables. Regression-based projection operators can also accommodate regularization by simply formulating a general cost function (Eq. (15)) with a regularization term. As such, we view the regression-based Mori–Zwanzig formalism as the most natural and accurate mathematical construct for NN-based learning methods [20, 21, 22, 23].

3 Numerical Analysis

3.1 An illustrative example: the Van der Pol oscillator

We now use the Van der Pol oscillator as an example to illustrate the regression-based learning of Mori–Zwanzig operators in action. The Van der Pol oscillator is a two-dimensional nonlinear system, which follows

$$\frac{d}{dt}\phi_1(t) = \mu \left(\phi_1 - \frac{\phi_1^3}{3} \right) - \phi_2, \quad (34a)$$

$$\frac{d}{dt}\phi_2(t) = \frac{1}{\mu}\phi_1. \quad (34b)$$

We chose $\mu = 1$ in this illustrative example. The Van der Pol oscillator has a globally stable limit cycle, which is a one-dimensional manifold embedded in the $\boldsymbol{\phi} = (\phi_1, \phi_2)$ -state space, as shown in Fig. 1(a). Note that we used the subscript of the state variable $\boldsymbol{\phi}$ to denote the component of the two-dimensional state, in contrast to the subscripts of the observables \mathbf{g}_n to denote the discrete-time (n) evolution of the vectorized observable, and $\mathbf{g}_{n,m}$ to denote the discrete-time (n) evolution of the m th observable. For illustrative purpose, we considered a single observable $g(\boldsymbol{\phi}) \triangleq \phi_1$ as the resolved dynamic variable. We used the `lsoda` integrator in `scipy.integrate.solve_ivp` to numerically simulate the two-dimensional system from an arbitrarily chosen initial state $\boldsymbol{\phi}_0 = (0, 1)$ and a relaxation time $t_c = 100$ for the system to relax to the limit cycle, whose period is roughly 6.663. We chose 50 initial conditions evenly sampled over one period; these initial conditions are also visualized in Fig. 1(a). Then, we collected snapshot data set \mathbf{D} by measuring $\phi_1(t)$ from $t = 0$ to $t = 20$ every $\Delta = 0.5$ from each of the initial conditions; two of the trajectories as shown in Fig. 1(b). In Figure 16(c)-(g), we show how the Mori's projection operator [11] is applied to the snapshot data set \mathbf{D} . In Figure 16(c), the paired samples are simply $x = \mathbf{D}(\cdot, 1, 1)$ and $y = \mathbf{D}(\cdot, 1, 2)$. That is, the x 's are the observed ϕ_1 at the time $t = 0$, and the $y^{(0)}$'s are the observed ϕ_1 one step ahead at the time $t = \Delta$. Because the system is not fully resolved, there can be two possible y 's for most of the measured x on the stable limit cycle (see Fig. 1(a)). Approximate Koopman and Mori's projector on a single observable is equivalent to a linear regression using $f(x; \theta) = \theta x$ to fit the data. The best-fit line is the projected model, $\theta_*^{(0)} x$. The slope of the best-fit model, $\theta_*^{(0)}$, is the approximate Koopman operator [14, 15, 16] and equivalently the 1×1 Markov transition matrix in the context of data-driven Mori–Zwanzig formalism [11]. After the first regression is made, the learned model $\theta_*^{(0)}$ is used to predict the system from $t = \Delta$ to 2Δ , and the residual $\mathbf{D}(\cdot, 1, 3) - \theta_*^{(0)} \mathbf{D}(\cdot, 1, 2)$ is assigned to $y^{(1)}$.

The next linear regression on the independent variable, which remains as $x = \mathbf{D}(\cdot, 1, 1)$, is performed (Fig. 1(d)), and the slope of the best-fit line is the first discrete-time 1×1 memory kernel [11]. The process repeats, and in Figs. 1(e-g), we showed the 5th, 10th, and the 30th linear regression. In Figs. (h-l), we used fifth-order nonlinear polynomial regression instead. As expected, the more expressive polynomial regression led to smaller errors than that of the linear regression.

Figures (m-o) shows the predictions of the learned models. First, we simulated the full system (34) from a different initial condition $\phi_0 = (1, 0)$ until $t = t_c = 100$ for relaxing the system to the stable limit cycle. Then, we measure $\phi_1(t + t_c; \phi_0)$ every $\Delta = 0.5$ until $t = 260$ as the ground truth of the dynamics. We considered three learned models that are more expressive than a single linear observable (ϕ), including and referred to as (1) the Mori (1) model: Mori’s projection with two polynomial functions as the observables, $\mathbf{g}(\phi) \triangleq [1, \phi_1]^T$; (2) the Mori (5) model: Mori’s projection with six lowest-order polynomial functions as the observables, $\mathbf{g}(\phi) \triangleq [1, \phi_1, \phi_1^2, \dots, \phi_1^5]^T$; (3) The nonlinear (5) model: a nonlinear regression-based projection operator based on fifth-order polynomial regression on a single observable $g(\phi) \triangleq \phi$. Given the snapshots in $t \in (100, 120)$, we used the truncated GLE Eq. (29) ($H = 1 + 20/0.5 = 41$) with $\mathbf{W}_{T \geq 41} := 0$ iteratively to predict the dynamics at $t \geq 120$. Figures 1(m) and (n) shows that the error due to the negligence of the orthogonal dynamics accumulates and eventually destabilize the prediction in Mori’s projection formalism. In contrast, Figure 1(o) shows that the nonlinear regression-based projection operator can reasonably approximate the true dynamics for a longer predictive horizon, using only the resolved snapshots.

We remark that this example was deliberately constructed as a minimal example. Our intention is to use a simple system and its transparent visualizations (Fig. 1) to illustrate the iterative learning of the Mori–Zwanzig operators in action. Little scientific insight and implications can be derived from this analysis.

3.1.1 Lorenz (1963) system

Our second example is the Lorenz ((1963)) model [30], which is a three-dimensional system

$$\frac{d}{dt}\phi_1(t) = \sigma(\phi_2 - \phi_1), \quad (35a)$$

$$\frac{d}{dt}\phi_2(t) = \phi_1(\rho - \phi_3) - \phi_2 \quad (35b)$$

$$\frac{d}{dt}\phi_3(t) = \phi_1\phi_2 - \beta\phi_3. \quad (35c)$$

We adopted the original model parameter values which E. Lorenz chose, $(\sigma, \rho, \beta) = (10, 28, 8/3)$. We again considered the “reduced-order model” as the $\phi_1(t)$ alone. A long trajectory with an arbitrarily selected initial condition $\phi_0^{\text{tr}} = (0.01, 1, 10)$ was generated using `scipy.integrate.solve_ivp` for data-driven learning. We discarded the initial transient before $t = t_c = 1000$, and collect 10^6 snapshots of ϕ_1 every $\Delta = 0.01$ until $t = t_c + 10^4$, as the samples on the strange attractor. A test trajectory was generated from a different initial condition $\phi_0^{\text{te}} = (0, 1, 2)$, and also with $t_c = 1000$.

We considered five projection operators and compared their performances, ordered by the

complexity (expressiveness) of the statistical model below. First, we again considered the Mori (1) projection operator, i.e., linear regression on the vectorized observable defined by $\mathbf{g}(\boldsymbol{\phi}) = [1, \phi_1]^T$. Without the memory effects, such a projection operator corresponds to the DMD analysis [14, 15]. Next, we considered the Mori (5) projection operator again, that is, linear regression on the vectorized observable which maps the full state $\boldsymbol{\phi}$ to $[1, \phi_1, \phi_1^2 \dots \phi_1^5]^T$. Without the memory, such a projection operator corresponds to an EDMD analysis [16]. The third projection operator we considered is a nonlinear fifth-order polynomial regression on ϕ_1 . Next, we considered a projection operator defined by a cubic (degree = 3) spline regression with ten knots (including boundary knots), evenly distributed between 1.5 times of the minimum and maximum of the collected ϕ_1 samples. After the spline features are generated, we performed a ridge regression with the L^2 -regularization parameter set at $\lambda = 10$. Finally, we considered a simple neural network. The architecture of the neural networks is two fully-connected feed-forward layers, each of which contains five artificial neurons, and a third linear layer with only one neuron. In this study, we always chose the hyperbolic tangent function as the activation function of the artificial neurons.

We used the measured snapshots to learn the operators $\boldsymbol{\Omega}^{(\ell)}$'s for each of the selected projection operators. Figure 2(a) shows the magnitude of the summary residual, defined as the averaged mean-squared error (MSE) of the best ℓ th regression model on the test trajectory. Recall that ℓ is the index of the memory terms (cf. Eq. (5)). Thus, we plotted the summary residual as a function of the physical time of the memory length ($\ell\Delta$) in Fig. 2(a). In addition, for linear Mori (and Koopman) models, the full optimization problem is the sum of the MSE of all the observables, in contrast to only the MSE of ϕ_1 in those nonlinear regression models. To make a consistent comparison, we only quantified and reported the MSE of the linear component ϕ_1 for Mori's projection operators in the figure. It is observed that with the increased complexity of the regression model, the residual with memory contribution can decrease significantly, from Mori (1) ($\approx 2 \times 10^{-1}$) to the expressive neural network ($\approx 2 \times 10^{-2}$). Note that without the memory contribution ($\ell = 0$), the magnitudes of the summary residual are indistinguishable; the significant improvement comes only with a finite-time memory contribution, ≈ 2.0 . This observation justified the advantage of the Mori–Zwanzig's memory-dependent formulation, especially for more expressive models.

To investigate the contribution of the memory effects, we plotted the L^2 -norm of the memory contribution in Eq. (5) ($\boldsymbol{\Omega}^{(\ell)}(\boldsymbol{\phi}(k\Delta + t_c; \boldsymbol{\phi}_0^{\text{te}}))$, $k = 0, 1, \dots, K + N$) averaged over the collected snapshots of the test trajectory. That is, we chose each snapshot along the long trajectory as a sample of the initial condition, and computed the memory contribution ℓ steps into the future. For Mori's projection operators, we only quantified the memory contributions to ϕ_1 , i.e., $\left[\boldsymbol{\Omega}^{(\ell)} \cdot \boldsymbol{\phi}(k\Delta + t_c; \boldsymbol{\phi}_0^{\text{te}}) \right]_2$ (note that the first component is the constant function 1). Figure 2(b) shows the memory contribution with various projection operators. We observed that memory contributions decayed as the memory index ℓ increased, regardless of the regression method. This observation suggests that a finite length (H) of the memory is sufficient, as the contribution of past history after a certain timescale would be small and negligible. As a result, in the following analysis, we chose a finite memory contribution by thresholding the squared L^2 -norm of the memory contribution at 10^{-7} . The corresponding memory lengths are: $H = 235$ snapshots for Mori (1); $H = 469$ snapshots for Mori (5); $H = 469$ snapshots for the nonlinear regression; $H = 469$ snapshots for the spline regression;

$H = 469$ snapshots for neural network.

After the memory kernels ($\Omega^{(\ell)}$) are learned, we turned our attention to the prediction of the learned models. We took the past history of the reduced-order variable $\phi_1(1000 \leq t \leq 1050)$ and use Eq. (29) to make predictions for $t > 1050$, assuming the orthogonal dynamics $\mathbf{W}_n = 0$. For comparison, we also made prediction from memory-less models, that is, setting $\Omega^{(\ell \geq 1)} = 0$. Note that the memory-less Mori (1) and Mori (5) corresponds to the approximate Koopman models [24].

Figure 3 shows the predicted trajectories by the learned models, using GLE (29). For all the methods, we found that the memory-less models failed to capture the characteristics of the resolved dynamics other than the long-time mean. For Mori (1) and Mori (5), a similar behavior of relaxation to the mean was observed. This should not be a surprise: as detailed in our recent work [11], Mori’s projection operator without the unresolved orthogonal dynamics is functionally identical to using the two-time correlation functions as the propagators for prediction. The two-time correlation function $\mathbf{C}_{i,j}(t)$ decays to 0 because the chaotic dynamics de-correlates at a large lag $t \gg 1$. Consequently, Mori (1) and (5) projection operators also made predictions that converge to the mean behavior in the long-time limit. They were able to predict the mean because a constant function 1, which can capture the constant bias, was included in the set of observables. Notably, Mori (1), Mori (5) with the memory kernels learned to predict a transient oscillation which crudely characterized the short-time dynamics of the Lorenz (1963) model. The drawback of the steady long-time prediction was significantly improved when we used nonlinear projection operators. The fifth-order polynomial regression showed a much better prediction in a short horizon, and an oscillation between the two wings of the Lorenz butterfly. Notably, the oscillation is not chaotic as it is in the fully resolved system. The prediction based on the spline regression, which is an intermediate model between the nonlinear polynomial regression and the NN-based regression models, began to exhibit chaotic behaviors in the long-time limit. Finally, the prediction of the one-dimensional reduced-order model based on an NN was qualitative similar to the chaotic dynamics of the fully-resolved Lorenz (1963) model.

To quantify the performance of the predictions, we first collected the long-time statistics by evolving Eq. (29) for 150,000 steps. We plotted the distributions of the collected trajectories based on the learned models in Fig. 4; such empirical distributions would be the stationary distribution if the process is ergodic. Clearly, Mori (1) and (5) showed an almost δ -like distribution at $\phi_1 = 0$ because their predictions converged to the mean in a finite timescale. All the nonlinear projection operators reasonably approximated the empirical distribution of ϕ_1 . We observed that the neural network out-performed the spline regression, which out-performed the plain fifth-order polynomial regression.

We further quantified the prediction error by the following metrics. First, we computed the squared L^2 -error of the prediction to the actual dynamics of $\phi_1(t)$. The initial condition and the histories were uniformly sampled along a long trajectory of the actual dynamics. We collected 25,000 samples and compute the mean-squared error as a function of the predictive horizon in Fig. 5(a). Within a short horizon, models with nonlinear projection operators made better predictions than Mori (1) and (5). The errors of the nonlinear models eventually grew larger at a finite predictive horizon ($t \approx 0.3$). We remark that, this should not be considered as a drawback but an advantage: beyond this timescale, Mori (1) and (5) predicted the mean of the chaotic dynamics, but nonlinear models predicted oscillatory solutions. In

terms of the mean squared error, predicting only the mean would have a smaller error. As such, we also computed the Kullback–Leibler divergence from the predictive distribution (approximated by the histogram of the samples from of the reduced-order models) to the ground truth distribution (approximated by the histogram of the samples from the actual dynamics), as shown in Fig. 5(b). With this metric, we observed that the reduced-order models based on the nonlinear projection operators captured the time-dependent distribution of ϕ_1 much better than the reduced-order models based on linear projection operators.

We conclude this section by discussing the potential pitfalls of nonlinear regression as the projection operator. Mainly, the stability of the learned models is not always guaranteed. We observed that the learned reduced model, provided some initial histories, can blow up in finite time. In Fig. 6, we plotted the deviation of the prediction from the actual dynamics. For each of the reduced-order models, we plotted 50 deviations, whose initial condition and histories sampled on a long ground-truth trajectory. We observed that the prediction the plain fifth-order polynomial regression could explode in finite time. The spline regression, which predicts constants outside the boundary knots seemed to alleviate the problem. However, when the prediction goes beyond the data distribution, the spline regression can also be “trapped” locally and induce high-frequency oscillations. Interestingly, we did not observe these pathologies in the neural network.

3.2 Kuramoto–Sivashinsky Equation

Our third example is the Kuramoto–Sivashinsky (KS) equation, which was developed in the 1970s for modeling instability of flame propagation [31, 32, 33]. Specifically, in this study, we considered the one-dimensional KS (partial differential) equation

$$0 = \frac{\partial}{\partial t}u(x, t) + \frac{\partial^2}{\partial x^2}u(x, t) + \frac{\partial^4}{\partial x^4}u(x, t) + u(x, t) \frac{\partial}{\partial x}u(x, t), \quad (36a)$$

for all time $t \geq 0$ on a bounded domain $x \in [0, L]$, given initial data $u(x, 0) = u_0(x)$. A periodic boundary condition was imposed, $u(t, 0) = u(t, L) \forall t$. We chose $L = 16\pi$ and uniformly discretized the space into $N = 128$ points. We used the pseudo-spectral fourth-order exponential time-derivative Runge–Kutta (ETDRK4) algorithm [34] with 2/3-dealiasing [24] to solve the spatially discretized system. The time step for the explicit ETDRK4 algorithm was set as 10^{-3} , and we collect the snapshots every 10^3 steps (so $\Delta = 1$). For the training data, we followed [34] and set $u_0^{\text{tr}}(x) = \cos(2\pi x/L) [1 + \sin(2\pi x/L)]$, and for the test data, $u_0^{\text{te}}(x) = \sin(2\pi x/L) [1 + \cos(2\pi x/L)]$. Both the training and the validation sets were simulated to $t = t_c + 10^5$, and we discarded the transient trajectories before $t_c = 5 \times 10^2$. For a reference, the Lyapunov time of the system is ≈ 12.56 [35].

We considered a four-fold reduced-order model by only observing the variable u every four discretized spatial grids. That is, $u(t, x_{4i})_i$, where $i = 0, 1, \dots, 31$ is the grid index. We augmented the reduced-order data set by two operations. (1.) *Shifting*: we used samples collected on different sub-grids: $u(t, x_{4i+j})$, $j = 0, 1, 2, 3$ and (2.) *Reordering*: we imposed the C_1 symmetry of the system, i.e., $u(t, x_{\text{mod}(4(i+k)+j, 32)})$, $k = 0, 1, \dots, 31$.

We also adopted and integrated the delay-embedding technique into some of the regression-based models. With the delay embedding, the input of the regression analysis is augmented to include a finite number, $E \in \mathbb{Z}_{\geq 0}$, of the current and past snapshots [29, 22]. As remarked

in the discussion in our previous study [11], the history dependence in the delay-embedding technique is not the memory effect in the Mori–Zwanzig formalism. We will provide a more detailed discussion in the Discussion section. For the rest of this article, we refer to the former as “delay-embedding” and the latter as “(MZ) memory effect” “(MZ) memory correction”, or simply “memory” in the figures. Our major aim of the analysis is to compare the performance of the models with delay-embedding and without MZ memory correction to those models with MZ memory correction but without delay-embedding.

We considered the following regression-based models and compared their performance. The first model is the linear Mori’s projection operator. Our preliminary analysis showed that a direct application of either data-driven Koopman [14] or Mori’s [11] on the snapshot observations $\{u(\cdot, x_{4i})\}_{i=0}^{31}$ performed poorly [data not reported]. Thus, we adopted the delay-embedding technique [29, 22] to augment the basis functions for learning the MZ kernels based on Mori’s projection operator. The model will be referred to as “Mori+DEm” model. Specifically, we use the past E snapshots to augment the input vector (which lives in \mathbb{R}^{32E}). For Mori’s projection operator, we chose a long embedding $E = 10$. We remark that the lowest-order result of the Mori’s projection operator (i.e., without the higher-order memory corrections, $\mathbf{\Omega}^{(\ell)}$, $\ell \geq 1$, in Eq. (5)) is functionally identical to the Hankel-DMD [29]. The second regression-based model was chosen to be a fully-connected neural network (FCNN). The architecture of the NN was two fully-connected layers, each of which contains 32 artificial neurons and a third linear layer with 32 outputs. The third regression-based projection operator was a convolutional neural network (CNN). CNNs are translationally invariant; such inductive bias is considered as beneficial for systems like KS equation, which are invariant under translations. The architecture of the CNN was two one-dimensional convolutional layers with five channels and kernel size of 11. The circular padding was implemented to impose the periodic boundary condition. As the fourth projection operator, we adopted the delay-embedding technique and used $E = 4$ past snapshots as the input for a CNN model, which will be referred as “CNN+DEm” model. In practice, the past E snapshots were stacked in the channel dimension of the input tensor of CNN. The architectures of the delay-embedded CNN model is identical to the one without the delay-embedding. This model will be referred to as the “CNN+DEm” model.

We used the snapshots collected along the long trajectory with the initial condition u_0^{tr} to learn the MZ kernels $\mathbf{\Omega}^{(\ell)}$ for each regression-based projection operators. For linear projection operators and for FCNN, we applied both the shifting and reordering data augmentation to impose the symmetries. For CNN’s, we applied only the shifting data augmentation. We sampled from the generated test trajectory to perform error analyses of the learned regression-based MZ kernels.

As a baseline reference for comparison, we performed reduced-order simulations. In these simulations, the reduced-order snapshots ($\{u_{t,x_{4i}}\}_{i=0}^{31}$) were treated as the full state of the KS-equation discretized on 32 spatially discretized grids (v. 128 of the ground-truth data-generation process). Each of the snapshots was evolved forward in time directly by the ETDRK4 integrator.

In Figure 7, we visualized the predictive trajectories and errors from the learned models, each with $\ell \leq 10$ MZ memory kernels. We chose $H = 10$ and used the truncated GLE (29) for making the predictions, again with the assumption $\mathbf{W}_n = 0$. Figures 7 (b, c) show the spatio-temporal evolution of the reduced-order simulation. Qualitatively speaking, we observed that

the reduced trajectory deviated from the “ground-truth” at a prediction horizon ≈ 20 , but it is capable of reproducing dynamical features that are visually indistinguishable. The Mori’s projected model with $E = 10$ delay-embedding (Figs. 7 (d, e)) quickly converged to the mean of the flow, as we expected. The FCNN model deviated from the “ground-truth” trajectory sooner than the reduced simulation did, but it also reproduced similar dynamical features; see Figs. 7 (f, g). Predictions from both CNN models deviated later than the reduced simulation did (Figs. 7 (h-k)). The $E = 4$ delayed-embedded CNN (Figs. 7 (j, k)) did not significantly improve the plain CNN (Figs. 7 (h, i)).

Quantitative error analysis of the regression models were performed with 15,000 trajectories uniformly sampled on the generated test trajectory. Figure 8(a) shows the normalized residual of the one-step prediction, defined as the mean squared error of the ℓ th-order MZ model, normalized by that of the Markovian model (i.e., only $\Omega^{(0)}$). The absolute error values are presented in the inset of Fig. 8(a). For all the regression models, including the MZ memory reduced the prediction error. We observed that the MZ memory effects can be captured with less than 10 memory kernels, justifying our choice of $H = 10$ for the predictive model. The plain CNN model without delay-embedding showed the highest percentage improvement by including the MZ memory. The delay-embedded CNN model had a slightly smaller percentage improvement in comparison to that of the plain CNN model, despite it has smaller absolute magnitude of mean squared error. The smaller absolute error of the $E = 4$ delay-embedded model is expected, as it is a more expressive model due to its larger input space, allowing coupling the delayed observables. Surprisingly, the plain CNN with $H = 4$ MZ contribution has a smaller absolute error than the $E = 4$ delay-embedded CNN (inset of Fig. 8(a)); see the Discussion Section for a detailed discussion. The FCNN model exhibited a much larger magnitude of error, and a smaller improvement from MZ memory contributions. Finally, as we expected, the linear Mori’s projection operator with delay-embedding had a very poor performance in one-step prediction.

We next focused on predictions at a further horizon. We set the furthest prediction horizon at $t = 100$, which is approximately 8 Lyapunov time. In Figure 8 (b), we compared the mean squared error as a function of the predictive horizon. It was observed that including the MZ memory improved the multistep predictions. Similar to the Lorenz ’63 system, at short prediction horizon ($\lesssim 20$), models with nonlinear projection operator performed much better than the linear Mori’s model. Among the nonlinear models, the FCNN model had worse predictions than the reduced simulation, and both the CNN models out-performed the reduced simulation. Comparing both CNN models, the delay-embedded CNN models performed better than the plain CNN at one-step prediction, as established in Fig. 8 (a). However, the CNN model overtook the time-embedding CNN model and became the best model—in the metric of the mean squared error—among all the considered models before the prediction horizon exceeded 55. As illustrated with the Lorenz (1963) model, the mean squared error is a less meaningful metric for the long-horizon predictions. As a second metric to quantify model performances, we used the Kullback–Leibler (KL) divergence from the regression-model predicted marginal distribution (u on a single grid) to that of the ground-truth (test trajectory) distribution. Because of the translational symmetry, we accumulated all the measured $u(t, x_{4i}), i = 0 \dots 31$, at different horizons for computing the empirical one-dimensional distributions of u . Figure 8 (c) shows the computed Kullback–Leibler divergence from the predicted distributions at different prediction horizon. Finally, we compared the

power spectra of based at the prediction horizon 100; Figure 9 also shows the spectrograms of the models with a single sampled initial condition. With these metrics, we concluded that the CNN models, with the MZ memory, performed much better than all other models and the reduced simulations over a long prediction horizon. Again, the presented evidence illustrated the advantage of nonlinear projection at predicting statistical properties of the dynamical system at a longer prediction horizon, despite the fact that sample-wise, the predicted trajectories deviate from the ground-truth trajectories.

The long-time marginal distribution of the regression-based models and the reduced simulation is shown in Figure 10. The empirical distributions were computed by accumulating measured u on each grid along long predicted trajectories (15,000 steps). The initial conditions of all the models, as well as the reduced simulation, were all set as u_0^{te} . Mori’s projection with delay-embedding showed almost δ -like distribution at the mean as expected, while the nonlinear models were capable of reproducing the stationary marginal distribution similar to the “ground-truth”. Among the nonlinear models, the distributions from both CNN models almost perfectly aligned with that of the test trajectory, while the FCNN model missed some finer details around the mean.

4 Discussion and Conclusion

The central proposition of this article is to adopt the regression analysis to define the projection operator in the Mori–Zwanzig formalism to enable data-driven learning of the operators. Given a set of sampled pairs of dependent and independent variables, a regression analysis identifies an optimal parametric function of the independent variables, such that the residuals are minimized in some norm, prescribed by the noise model. In the context of dynamical systems, the dependent variables are the future observations, and the independent variables are the present ones. When the system is not fully resolved, the future observations can not always be uniquely determined by the present ones due to missing information of the unresolved degrees of freedom. Consequently, future observations can be a one-to-many mapping of the present ones in under-resolved systems. A regression projects such one-to-many mapping to a one-to-one or many-to-one function, constrained by the data. It is a projection operator because an additional regression analysis on the samples drawn from the best-fit model results in the best-fit model, satisfying the definition of a projection operator $\hat{\mathcal{P}}: \hat{\mathcal{P}}^2 = \hat{\mathcal{P}}$.

To identify regression analysis as a projection operator is not a novel idea; it is an established concept in statistics. For example, see [36] for linear regression as an orthogonal projection, and [37] for regularized regression in terms of the Reproducing Kernel Hilbert Space. The notion of the decomposing the samples of the dependent variables into a regressional and an orthogonal component [38] even went back to Kolmogorov in the 1940s [39]. The major conceptional contribution of this manuscript is the proposition to adopt a regression analysis as *the* projection operator in the Mori–Zwanzig formalism.

We showed that the special choice of adopting linear regression models results in our previously proposed data-driven learning algorithm for the MZ formalism with Mori’s projection operator [11]. Thus, the proposed regression-based projection operator is a generalization of our previous proposition. Our proposed procedure to extract the MZ memory kernels

is readily applicable to a large set of data-driven learning methods for dynamical systems in the literature because they can be cast into the form of Eqs. (15)-(18). For example, approximate Koopman methods with neural-network-based learning of the functional bases with ridge and sparsity-induced regularizations [20, 21, 22, 23], and Sparse Identification of Nonlinear Dynamics [19, 40]. We remark that these data-driven learning methods often implicitly assume that the system is fully resolved without missing information. Should it be the case and should the regression model be expressive enough, our procedure would lead to a perfect Markov model $\Omega^{(0)}$ that leaves zero residuals. Our interest, as well as the setup of the Mori–Zwanzig formalism, is on partially resolved dynamical systems. In general, when a system is not fully resolved and when there exists interaction between the resolved and unresolved dynamics, MZ memory kernels and orthogonal dynamics naturally emerge. The major computational contribution of this manuscript is to provide a principled algorithm, motivated by the structure of the Generalized Langevin Equation (5), for extracting these higher-order corrections, given any regression model as the projection operator. To the authors’ knowledge, such an intuitive, yet elegant procedure does not currently exist in the literature of the Mori–Zwanzig formalism.

Regression-based MZ methods can fill in the gap between the existing Mori’s and Zwanzig’s projection operators, which can be respectively considered as the simplest and the most optimal projection operator [3]. Our proposition significantly broadens the applicability of the Mori–Zwanzig formalism, because the complexity of the regression model can be gradually adjusted between these two extremes. Ranked by the complexity of the regression analysis, we examined and presented the linear regression analysis on linear functional basis (DMD) or nonlinear functional basis (EDMD), nonlinear polynomial regression, spline regression with ridge regularization, and the more modern and expressive neural network architectures such as FCNN and CNN for performing nonlinear regression. With a finite snapshot data set, it may not be computational feasible to learn the operators with the most optimal Zwanzig’s projection operator, because it requires estimating the conditional expectation functions (e.g, $f(X) := \mathbb{E}[Y|X]$). A finite set of data may not be sufficient to cover all possible condition X , let along the large amount of samples of Y needed for estimating the expectation value. Instead, regression analysis identifies the best fit among a family of functions to approximate the conditional expectation function. When the family of functions is expressive enough to include the conditional expectation function, our regression-based MZ would converge to the Zwanzig’s projection operator in the infinite-data limit. As neural networks are universal function approximators [41], we hypothesize that the MZ formalism with the optimal Zwanzig projection operator can be reasonably realized by a neural-network-based regression. Indeed, in our numerical experiments, we observed the superiority of those regression models based on neural networks.

Mathematically, the presented method learns the *operators* $\Omega^{(\ell)}$, which maps measurable functions to measurable functions, in Eq. (7). Computationally, this is made possible by using the regressional functions to model the *functions* $\Omega^{(\ell)}$ in Eq. (5), given snapshots of the observations $\mathbf{g}(\phi(t))$, where the state is sampled from the induced distribution $\phi(t) = \phi(t; \phi_0)$, $\phi_0 \sim \mu$. It should be noted that (machine) learning of functional operators is not a new idea. For example, Li et al. [42] recently laid out a general ML architecture (DeepONet) for learning nonlinear functional operators, relying on a universal approximation theorem proved in the 1990s [43]. Another example is the approximate Koopman learning methods

[14, 15, 16], with which one aims to learn the (approximate) Koopman operator, linearly mapping functions to functions. With these methods, samples of function evaluations must be provided for supervised learning of the operators. Where the functions are evaluated—where the “sensors” are in the language of [42]—requires human inputs. With regard to our aim of learning dynamical systems, analogously, we also need to specify the initial distribution μ . What is different from the general DeepONet [42] is that we can rely on the dynamics to naturally propagate the specified initial distribution to a future time $\phi(t)$, with which the samples of the observations can be generated for supervised learning—in our case, a general regression problem.

We have been framing the above discussions in terms of data-driven learning methods. In fact, our original desire for developing data-driven MZ methods with nonlinear projection operators emerged from *modeling* reduced-order dynamical systems. Devising closure schemes is not only necessary but also critical in these modeling endeavors, especially for multiscale models. Based on our knowledge, there are very few linear closure schemes which resemble the linear projection operators (i.e., approximate Koopman [14, 16] and data-driven Mori [11]), which are not generalizable to accommodate nonlinear closure schemes. As illustrated in Sec. 2.13, the proposed nonlinear regression-based MZ formalism can connect to existing reduced-order models. In the future, we intend to devise nonlinear regression models based on the structure of existing closure schemes. The operational logic is that, despite a purely data-driven (black-box) approach could work, our numerical experiments suggested that this approach is extremely data-hungry. Contrarily, a modeling (white-box) approach requires no data, but only works in a limited scope. We argue the optimal way forward is to inject known structures into the learning architecture, and use the data to parametrize the reduced-order models. With this (gray-box) approach, we are formally injecting inductive biases, which have been pointed out as the critical component for a successful scientific machine learning [42].

In this article, we are primarily interested in the quality of multistep predictions of the learned reduced-order models. We showed that despite linear regression models outperformed nonlinear ones at the far horizon, it is only because the linear models predicted the mean of the dynamics. Because linear models fully ignore higher-order statistical properties of the dynamical systems, we are not confident that such “coarse-grained dynamical systems” are the proper way forward for making predictions. Although such a problem for linear projection operators does not exist when a set of observables linearly spanned an invariant Koopman space, it is extremely difficult to identify the invariant Koopman space in practice. It is our perspective that developing nonlinear projection operator methods is a practical and promising way forward for predictive coarse-grained models. We do remark that methods based on linear projection operators are ideal for estimating the Koopman eigenvalues and eigenfunctions, and the globally convex learning problem is easier, provided a set of linearly independent observables. We should also remark that nonlinear regression is not always advantageous in making predictions. As we witnessed in the Lorenz (1963) model, despite a learned nonlinear regression model could improve predictive accuracy within a finite horizon, sometimes these nonlinear closure methods lose long-term stability (Fig. 5). Such a pathology is model- and horizon-dependent, and interestingly, not observed when we used neural-network-based regression.

With the Kuramoto–Sivashinsky model, we also compared the delay-embedding and the

memory effect of the Mori–Zwanzig formalism. Our motivation was to provide clarification on a pervasive confusion between these two memory-dependent theories. Such a confusion emerged from a false presumption that all memory-dependent theories are equivalent. We also provided numerical results based on respective data-driven learning methods.

Because the memory effect in Mori–Zwanzig formalism is due to the interaction between the resolved and unresolved dynamics, the memory kernels and the orthogonal dynamics must satisfy the stringent Generalized Fluctuation Dissipation relation (Eq. (11)), which depends on the choice of the resolved observables and the projection operator. Guided by the GFD (11), learning MZ operators can be decomposed into H smaller regression (optimization) problem in M dimensions. Notably, the MZ memory contribution is always a linear sum of memory kernels evaluated at each past snapshot (Eq. (5)). The formalism excludes coupling between the observations made at different times, for example, $\mathbf{g}_{n_1, m_1} \times \mathbf{g}_{n_2, m_2}$, with $n_1 \neq n_2$. This is because the projection operator \mathcal{P} is applied at each time by construction. The functional space that \mathcal{P} is projected into is those regressional functions $f(\cdot; \theta)$, which always only depend on M reduced-order observables evaluated at a specific time.

On the contrary, for delay-embedding, the domain of the functions is augmented to include E past snapshots of M reduced-order observables. The learning is a global regression (optimization) problem in an $M \times E$ -dimensional functional space. The motivation of delay-embedding is that the past history may contain useful information for inferring the unresolved dynamics. Because such an augmented functional space ($M \times E$) is larger than the fixed (M) operational space in the Mori–Zwanzig formalism, delay-embedding can be considered as a more expressive regression model. Let us denote the past E snapshots of the observables $\mathbf{g}_{0, -1 \dots -E+1}$ by a flattened vector $\mathbf{g}_{0: -E+1}(\boldsymbol{\phi}_{-T}) \in \mathbb{R}^{ME}$. Formally, delay embedding can be considered as a regression to identify the optimal function $\mathbf{f}_{\theta^*}(\mathbf{g}_{0: -E+1}(\boldsymbol{\phi}_{-T}))$ that best approximates $\mathbf{g}_1(\boldsymbol{\phi}_0)$. As such, coupled terms could exist, should the family of regressional functions admits, within the delay-embedding paradigm. Hankel-DMD [29] is the special delay-embedding case that the learning is formulated as a linear regression problem, i.e., the regression functions take the form $\mathbf{f}(\mathbf{g}_{0: -E+1}(\boldsymbol{\phi}_0); \boldsymbol{\beta}) := \boldsymbol{\beta} \cdot \mathbf{g}_{t-E+1:t}(\boldsymbol{\phi}_0)$, where $\boldsymbol{\beta}$ is an $(ME) \times (ME)$ matrix (v. in linear regression-based MZ, $\boldsymbol{\beta}^{(\ell)}$ is $M \times M$, $\ell = 0 \dots H - 1$ with the same memory length). Although its structure resembles Mori–Zwanzig’s Generalized Langevin Equation with Mori’s linear projection operator, it is not necessary—and generally not the case—that the best-fit parameters of the Hankel-DMD satisfy the Generalized Fluctuation-Dissipation relation 11.

The structure of the Generalized Langevin Equation is contained in the family of delay-embedded regressional functions, so the error of the former should have been lower-bounded by that of the latter. However, with the Kuramoto–Sivashinsky equation, we showed that the Mori–Zwanzig formalism with $H = 4$ truncated memory contribution out-performed the more expressive delay-embedded CNN with $E = 4$. We hypothesized that it was because the architecture of the delay-embedded CNN was not as expressive as the CNN with MZ memory. As the latter contained four separate CNNs, each of which learned an operator $\boldsymbol{\Omega}^{(\ell)}$, the delay-embedded CNN had a fixed architecture (the past history augmented the channel dimension of the input and not the complexity of the regression model). To examine whether a more expressive delay-embedded CNN could learn better, we deliberately developed delay-embedded CNNs whose number of parameters are identical to H times the number of parameters CNNs

for learning MZ operators. For $H = E = 4$, we still observed that the MZ out-performed the delay-embedding model (1-step MSE of the CNN+MZ: 1.563×10^{-5} ; 1-step MSE of the CNN+DEm: 2.038×10^{-5}). For $H = E = 10$, the delay-embedding model performed better in predicting the first step than the MZ did (1-step MSE of the CNN+MZ: 1.478×10^{-5} ; 1-step MSE of the CNN+DEm: 1.085×10^{-5}). However, for multistep predictions, MZ out-performed the delay-embedding after a few ($\mathcal{O}(10)$) steps, see Fig. 11. These observations highlight the practical difficulty of learning the larger delay-embedded models: they require more data, potentially need a longer history, and for nonlinear problems, the training could be trapped in some local minimum. The precise reason why the delay-embedded models are worse in predicting multiple steps into the future merits a future, more carefully designed investigation.

It is important to point out that Mori–Zwanzig formalism and delay embedding are not mutually exclusive. On the Kuramoto–Sivashinsky model, we illustrated a delay-embedded CNN combined with the MZ formalism. In this combined approach, the input of the Markov operator was a flattened observable $\mathbf{g}_{0:-E+1}$, and the input of the ℓ th-order ($\ell \geq 1$) memory operator was a vector function of the flattened observable shifted by ℓ time step, $\mathbf{g}_{-\ell:-E-\ell+1}$. We showed in Fig. 8(a) and (b) that the inclusion of the MZ memory operators can further improve the performance of the delay-embedded CNN.

We view regression-based Mori–Zwanzig formalism as a promising direction to enable data-driven learning for partially observed dynamical systems. We have identified a few directions which merit further investigation. Theoretically, we would like to generalize the formalism for stochastic systems, including generic stochastic processes, Hidden Markov Models, and random dynamical systems. As an application, we are working on the application of the NN-based Mori–Zwanzig models on isotropic turbulence data [12]. Another interesting idea we would like to explore is making formal connections to time-series analysis. As recently pointed out, Dynamic Mode Decomposition can be considered as a Vector Autoregression (VAR-1) model in time-series analysis [44]. It is clear that the Hankel-DMD can be mapped to a VAR- p model in time-series analysis. It was shown that the Wiener projection can be mapped to the nonlinear autoregressive moving average model with exogenous inputs (NARMAX) in time-series analysis, after a rational approximation in the Laplace domain [24]. These existing evidence prompted an interesting research question: what is the time-series analysis method which corresponds to the MZ formalism, which imposes a very stringent GFD condition on the residuals and the memory? Next, we discussed the difference between the memory-embedding techniques such as Hankel-DMD and the MZ formalism. These two formalisms can be considered as two extremes of memory-dependent dynamics: The former considers an extremely large functional space which couples a whole segment of the past trajectory, and the latter restricts its functional space to the regressional functions at an instantaneous time. In modern machine learning for time series, Recurrent Neural Networks with Long Short-Term Memory (RNN-LSTM) [45] and its variants are also equipped with memory kernels, learned by a neural network. It will be an interesting direction to investigate whether RNN-LSTM functions more similarly to the time-embedding or to the MZ formalism. Finally, in this manuscript, we did not attempt to model the orthogonal dynamics, which is needed for making accurate predictions. Our test showed that the common choice of white (independent in time) Gaussian noise is unsatisfactory (data not shown). A certain color-noise must be needed. This is because the orthogonal dynamics,

which encode unresolved dynamics, are also correlated in time. Despite that our numerical extraction of the orthogonal dynamics provides the data stream for learning, how one models the orthogonal dynamics in a principled and system-agnostic way remains an open and challenging problem.

Acknowledgement

YTL was primarily supported by the Laboratory Directed Research and Development (LDRD) Project “Uncertainty Quantification for Robust Machine Learning” (20210043DR). YT, DP and YTL were also supported by the LDRD project “Accelerated Dynamics Across Computational and Physical Scales” (20220063DR). DL was partially supported by the LDRD project “MASS-APP: Multi-physics Adaptive Scalable Simulator for Applications in Plasma Physics” (20220104DR).

References

- [1] Mori H. Transport, Collective Motion, and Brownian Motion. *Progress of theoretical physics*. 1965;33(3):423-55.
- [2] Zwanzig R. Nonlinear Generalized Langevin Equations. *Journal of Statistical Physics*. 1973;9(3):215-20.
- [3] Alexandre J Chorin, Hald OH, Kupferman R, Chorin AJ, Hald OH, Kupferman R. Optimal Prediction with Memory. *Physica D: Nonlinear Phenomena*. 2002 Jun;166(3-4):239-57.
- [4] Parish EJ, Duraisamy K. A Dynamic Subgrid Scale Model for Large Eddy Simulations Based on the Mori–Zwanzig Formalism. *Journal of Computational Physics*. 2017 Nov;349:154-75.
- [5] Parish EJ, Duraisamy K. Non-Markovian Closure Models for Large Eddy Simulations Using the Mori–Zwanzig Formalism. *Phys Rev Fluids*. 2017 Jan;2(1):14604.
- [6] Okamura M. Validity of the essential assumption in a projection operator method. *Physical Review E*. 2006;74(4):046210.
- [7] Mori H, Okamura M. Dynamic structures of the time correlation functions of chaotic nonequilibrium fluctuations. *Physical Review E*. 2007;76(6):061104.
- [8] Meyer H, Pelagejcev P, Schilling T. Non-Markovian out-of-equilibrium dynamics: A general numerical procedure to construct time-dependent memory kernels for coarse-grained observables. *EPL (Europhysics Letters)*. 2020;128(4):40001.
- [9] Maeyama S, Watanabe TH. Extracting and modeling the effects of small-scale fluctuations on large-scale fluctuations by Mori–Zwanzig projection operator method. *J Phys Soc Jpn*. 2020;89(2):024401.

- [10] Meyer H, Wolf S, Stock G, Schilling T. A numerical procedure to evaluate memory effects in non-equilibrium coarse-grained models. *Adv Theory Simul.* 2021;4(4):2000197.
- [11] Lin YT, Tian Y, Livescu D, Anghel M. Data-Driven Learning for the Mori–Zwanzig Formalism: A Generalization of the Koopman Learning Framework. *SIAM Journal on Applied Dynamical Systems.* 2021 Jan;20(4):2558-601.
- [12] Tian Y, Lin YT, Anghel M, Livescu D. Data-Driven Learning of Mori–Zwanzig Operators for Isotropic Turbulence. *Physics of Fluids.* 2021 Dec;33(12):125118.
- [13] Rowley CW, Mezić I, Bagheri S, Schlatter P, Henningson DS. Spectral Analysis of Nonlinear Flows. *Journal of Fluid Mechanics.* 2009;641:115-27.
- [14] Schmid PJ. Dynamic Mode Decomposition of Numerical and Experimental Data. *Journal of Fluid Mechanics.* 2010;656:5-28.
- [15] Schmid PJ, Li L, Juniper MP, Pust O. Applications of the Dynamic Mode Decomposition. *Theoretical and Computational Fluid Dynamics.* 2011 Jun;25(1):249-59.
- [16] Williams MO, Rowley CW, Kevrekidis IG. A Data–Driven Approximation of the Koopman Operator : Extending Dynamic Mode Decomposition. *Journal of Nonlinear Science.* 2015;25(6):1307-46.
- [17] Durbin P. Some recent developments in turbulence closure modeling. *Annual Review of Fluid Mechanics.* 2018;50:77-103.
- [18] Majda AJ, Wang X. *Nonlinear dynamics and statistical theories for basic geophysical flows.* Cambridge University Press; 2006.
- [19] Brunton SL, Proctor JL, Kutz JN. Discovering governing equations from data by sparse identification of nonlinear dynamical systems. *Proceedings of the National Academy of Sciences.* 2016;113(15):3932-7.
- [20] Li Q, Dietrich F, Bollt EM, Kevrekidis IG. Extended Dynamic Mode Decomposition with Dictionary Learning: A Data-Driven Adaptive Spectral Decomposition of the Koopman Operator. *Chaos: An Interdisciplinary Journal of Nonlinear Science.* 2017 Oct;27(10):103111.
- [21] Yeung E, Kundu S, Hodas NO. Learning Deep Neural Network Representations for Koopman Operators of Nonlinear Dynamical Systems. 2019 American Control Conference (ACC). 2017:4832-9.
- [22] Lusch B, Kutz JN, Brunton SL. Deep Learning for Universal Linear Embeddings of Nonlinear Dynamics. *Nature Communications.* 2018;9(1).
- [23] Wehmeyer C, Noé F. Time-Lagged Autoencoders: Deep Learning of Slow Collective Variables for Molecular Kinetics. *The Journal of Chemical Physics.* 2018;148(24):241703.
- [24] Lin KK, Lu F. Data-Driven Model Reduction, Wiener Projections, and the Koopman–Mori–Zwanzig Formalism. *Journal of Computational Physics.* 2021 Jan;424:109864.

- [25] Gerlich G. Die Verallgemeinerte Liouville-Gleichung. *Physica*. 1973 Nov;69(2):458-66.
- [26] Zwanzig R. *Nonequilibrium Statistical Mechanics*. Oxford ; New York: Oxford University Press; 2001.
- [27] Darve E, Solomon J, Kia A. Computing Generalized Langevin Equations and Generalized Fokker-Planck Equations. *Proceedings of the National Academy of Sciences*. 2009 Jul;106(27):10884-9.
- [28] Koopman BO, v Neumann J. Dynamical Systems of Continuous Spectra. *Proceedings of the National Academy of Sciences*. 1932;18(3):255-63.
- [29] Arbabi H, Mezić I. Ergodic Theory, Dynamic Mode Decomposition, and Computation of Spectral Properties of the Koopman Operator. *SIAM Journal on Applied Dynamical Systems*. 2017;16(4):2096-126.
- [30] Lorenz EN. Deterministic Nonperiodic Flow. *Journal of Atmospheric Sciences*. 1963;20(2):130-41.
- [31] Kuramoto Y. Diffusion-Induced Chaos in Reaction Systems. *Progress of Theoretical Physics Supplement*. 1978 Feb;64:346-67.
- [32] Sivashinsky GI. On Flame Propagation under Conditions of Stoichiometry. *SIAM Journal on Applied Mathematics*. 1980;39(1):67-82.
- [33] Sivashinsky GI. Nonlinear Analysis of Hydrodynamic Instability in Laminar Flames—I. Derivation of Basic Equations. *Acta Astronautica*. 1977;4(11):1177-206.
- [34] Kassam AK, Trefethen LN. Fourth-Order Time-Stepping for Stiff PDEs. *SIAM Journal on Scientific Computing*. 2005 Jan;26(4):1214-33.
- [35] Edson RA, Bunder JE, Mattner TW, Roberts AJ. Lyapunov Exponents of the Kuramoto–Sivashinsky PDE. *The ANZIAM Journal*. 2019;61(3):270-85.
- [36] Deisenroth MP, Faisal AA, Ong CS. *Mathematics for Machine Learning*. Cambridge University Press; 2020.
- [37] Nosedal-Sanchez A, Storlie CB, Lee TC, Christensen R. Reproducing kernel Hilbert spaces for penalized regression: A tutorial. *The American Statistician*. 2012;66(1):50-60.
- [38] Afriat SN. In: *Regression and Projection*. Berlin, Heidelberg: Springer Berlin Heidelberg; 1969. p. 277-301.
- [39] Kolmogorov AN. On the proof of the method of least squares. *Uspekhi Mat Nauk*. 1946;1(1 (11)):57-70.
- [40] Kaheman K, Kutz JN, Brunton SL. SINDy-PI: a robust algorithm for parallel implicit sparse identification of nonlinear dynamics. *Proceedings of the Royal Society A: Mathematical, Physical and Engineering Sciences*. 2020;476(2242):20200279.

- [41] Murphy KP. Machine Learning: A Probabilistic Perspective. MIT press; 2012.
- [42] Lu L, Jin P, Pang G, Zhang Z, Karniadakis GE. Learning Nonlinear Operators via DeepONet Based on the Universal Approximation Theorem of Operators. Nature Machine Intelligence. 2021 Mar;3(3):218-29.
- [43] Tianping Chen, Hong Chen. Universal Approximation to Nonlinear Operators by Neural Networks with Arbitrary Activation Functions and Its Application to Dynamical Systems. IEEE Transactions on Neural Networks. 1995 Jul;6(4):911-7.
- [44] Bollt E. On Explaining the Surprising Success of Reservoir Computing Forecaster of Chaos? The Universal Machine Learning Dynamical System with Contrast to VAR and DMD. Chaos: An Interdisciplinary Journal of Nonlinear Science. 2021 Jan;31(1):013108.
- [45] Hochreiter S, Schmidhuber J. Long Short-Term Memory. Neural Comput. 1997;9(8):1735-80. Available from: <https://doi.org/10.1162/neco.1997.9.8.1735>.

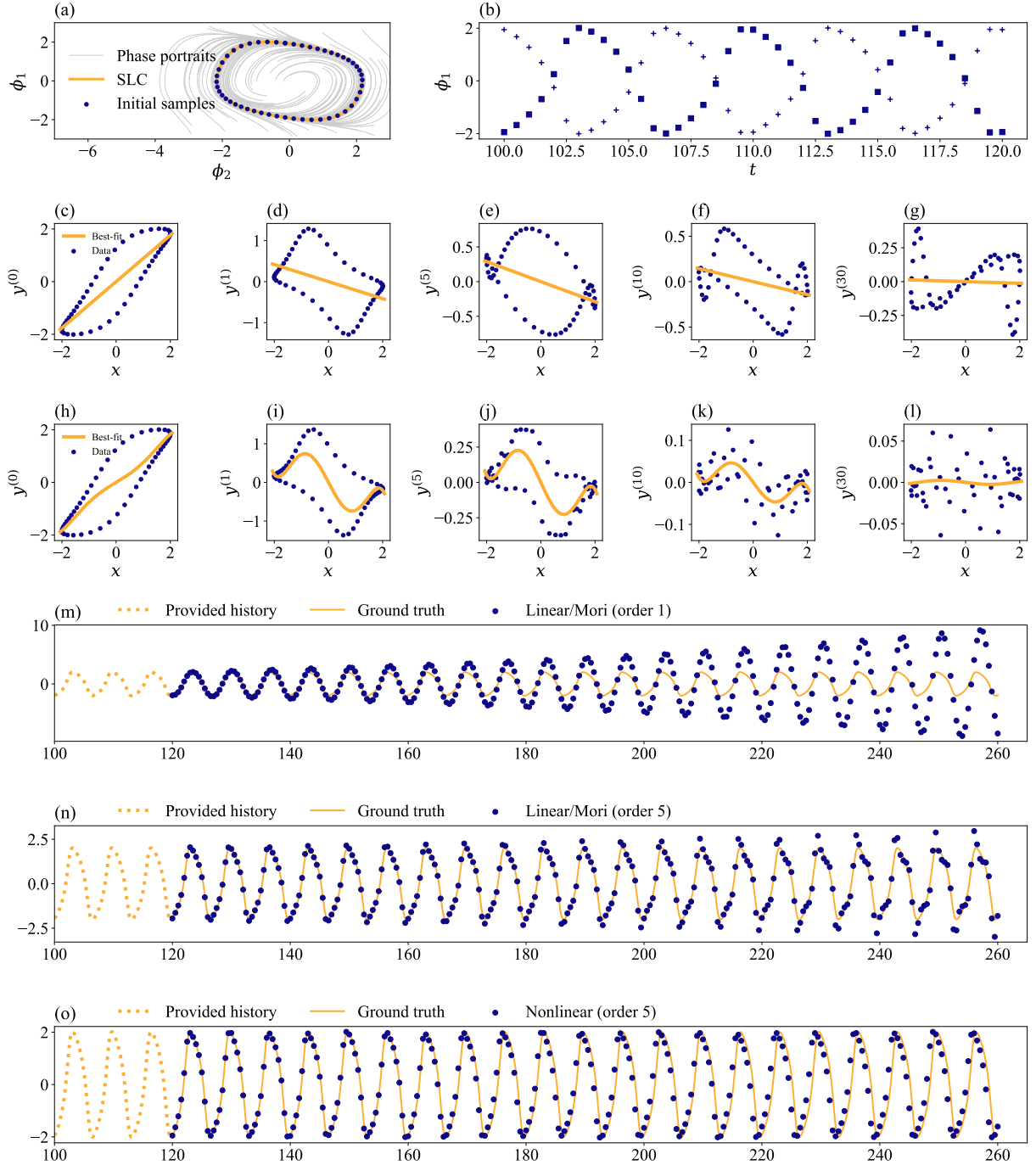


Figure 1: The Van der Pol oscillator. (a) The phase portraits of the full system, the stable limit cycle (SLC), and the initial samples of the data matrix $\mathbf{D}(\cdot, 1, 1)$; (b) Snapshot samples along two trajectories, $\mathbf{D}(1, 1, \cdot)$ and $\mathbf{D}(26, 1, \cdot)$; (c-g) Linear regression with a single observable, $f(x; \theta) := \theta x$; (h-l) Nonlinear polynomial regression with a single observable, $f(x; \theta) := \sum_{i=0}^5 \theta_i x^i$; (m-o) Prediction of the learned (m) linear regression with two polynomial basis function up to order 1, $\mathbf{g}(\phi) \triangleq [1, \phi]^T$, (n) linear regression with polynomial basis function up to order 5, $\mathbf{g}(\phi) \triangleq [1, \phi, \phi^2, \dots, \phi^5]^T$, and (o) nonlinear polynomial regression of a single observable ($g(\phi) \triangleq \phi$) up to order 5.

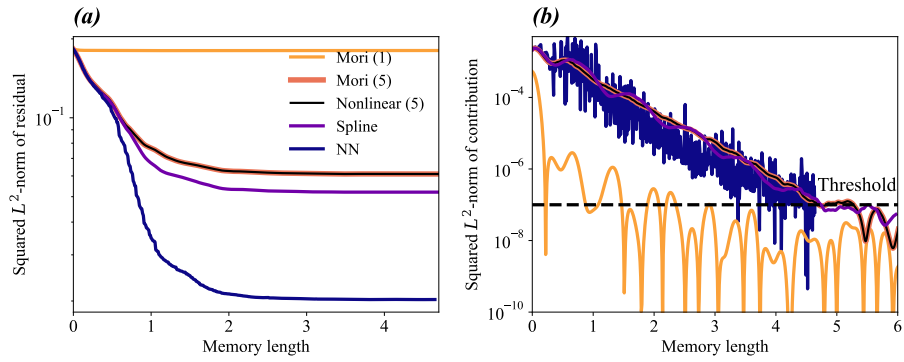


Figure 2: The Lorenz (1963) system. (a) The squared L^2 -norm of the validation residual as the memory length increases. (b) The squared L^2 -norm contribution at different memory length. The threshold is set at 10^{-7} for determining the memory length. Note that in these visualizations, Mori (5) and Nonlinear (5) are identical. The memory length is in the physical time unit, i.e., memory length 1 corresponds to 100 discrete-time steps ($\Delta = 0.01$).

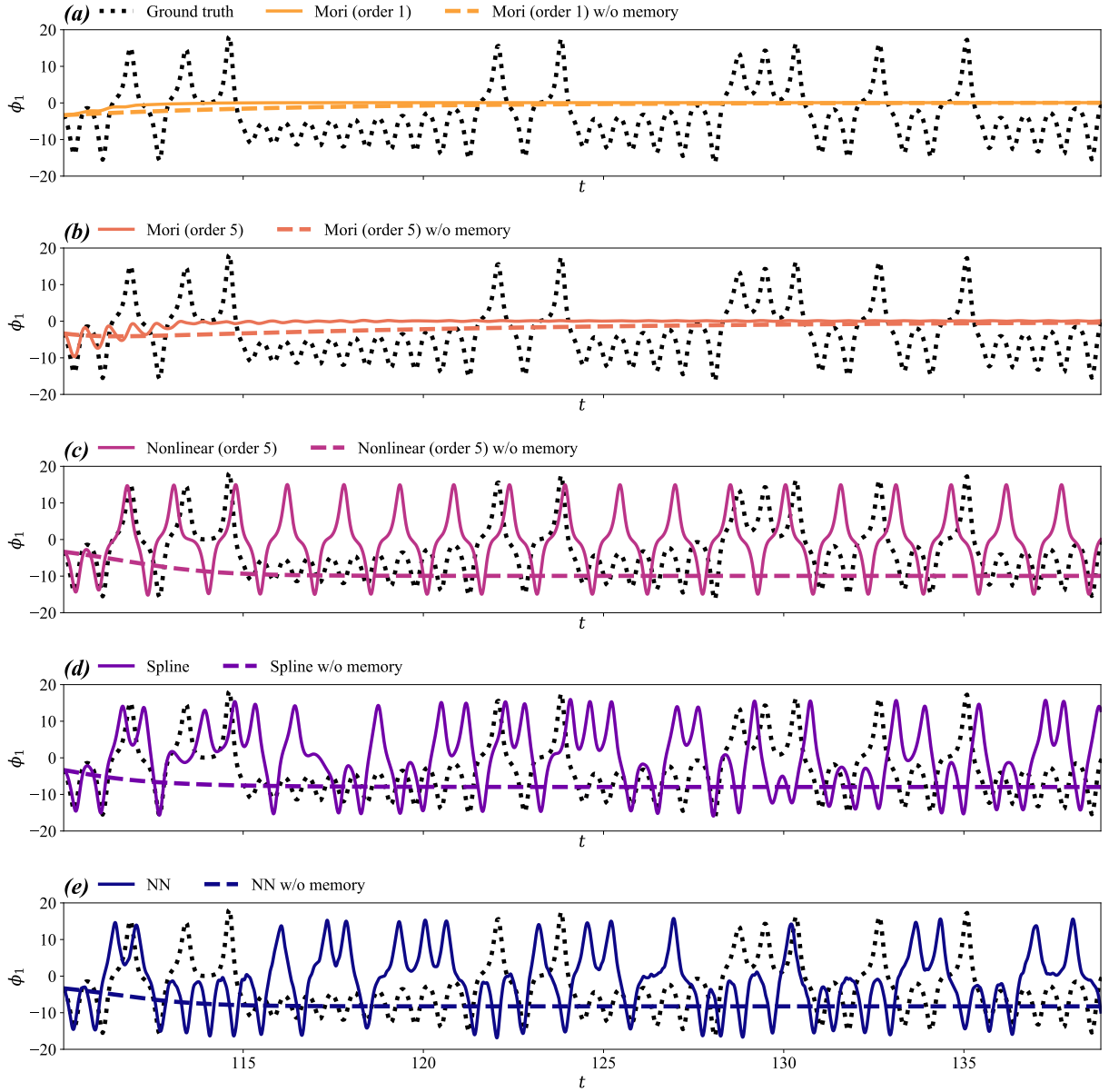


Figure 3: The Lorenz (1963) system. The predicted trajectories for the learned models based on (a) Mori (1) projection operator, (b) Mori (5) projection operator, (c) a projection by fifth-order polynomial regression on ϕ_1 , (d) a projection by ridge and spline regression, and (e) a projection by a neural network (NN).

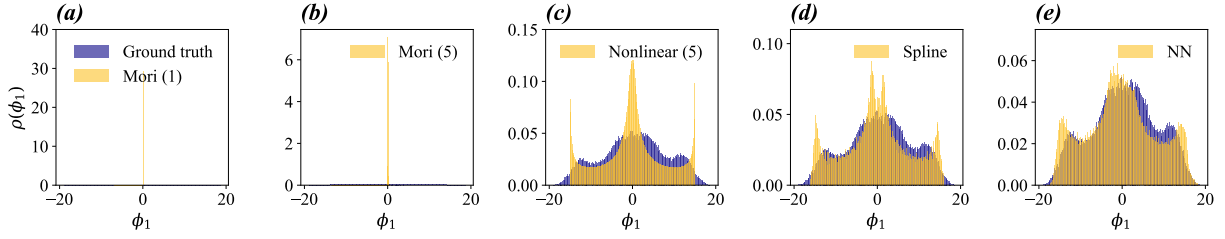


Figure 4: Long-time statistics of the MZ model predictions of the Lorenz (1963) model.

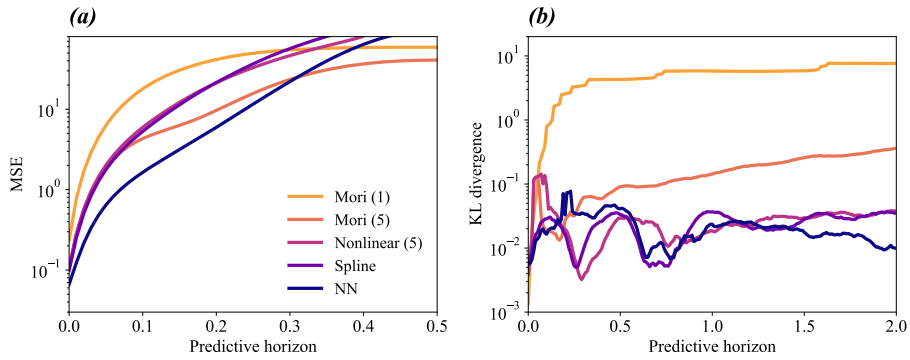


Figure 5: Error of the reduced-order models on the Lorenz (1963) system. (a) The mean squared error of the prediction as a function of the predictive horizon; (b) the Kullback–Leibler divergence of the empirical distribution from the model predicted distribution as a function of the predictive horizon.

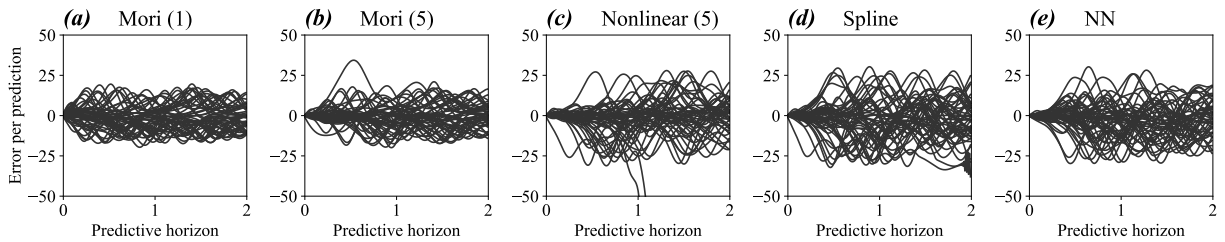


Figure 6: The Lorenz (1963) system. (a-e) The deviation of 50 predicted trajectories using the learned models.

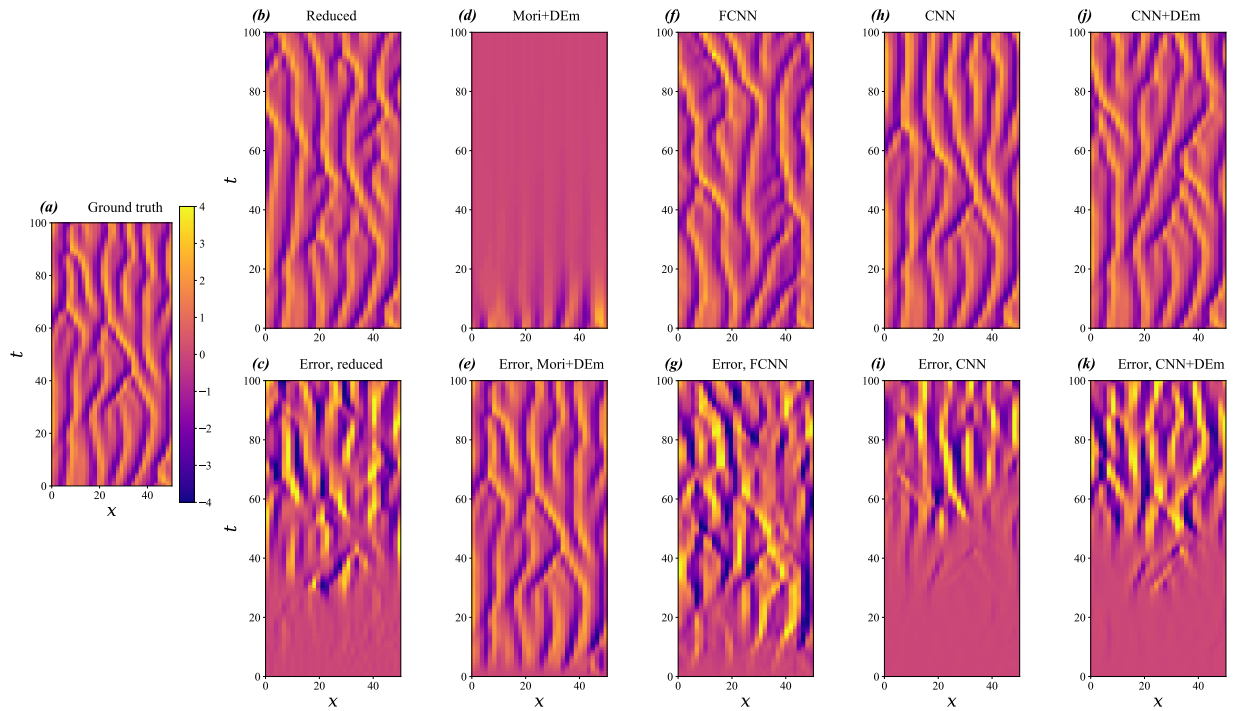


Figure 7: Regression-based Mori-Zwanzig learning of Kuramoto–Sivashinsky equation. (a) “Ground-truth” reduced-order observation. (b, d, f, h, j) Predicted trajectories using reduced-order simulation and four regression based Mori–Zwanzig models and (c, e, g, i, k) error of the predicted trajectories. The x - and y -axis of panels (b-k) are identical to those in the panel (a).

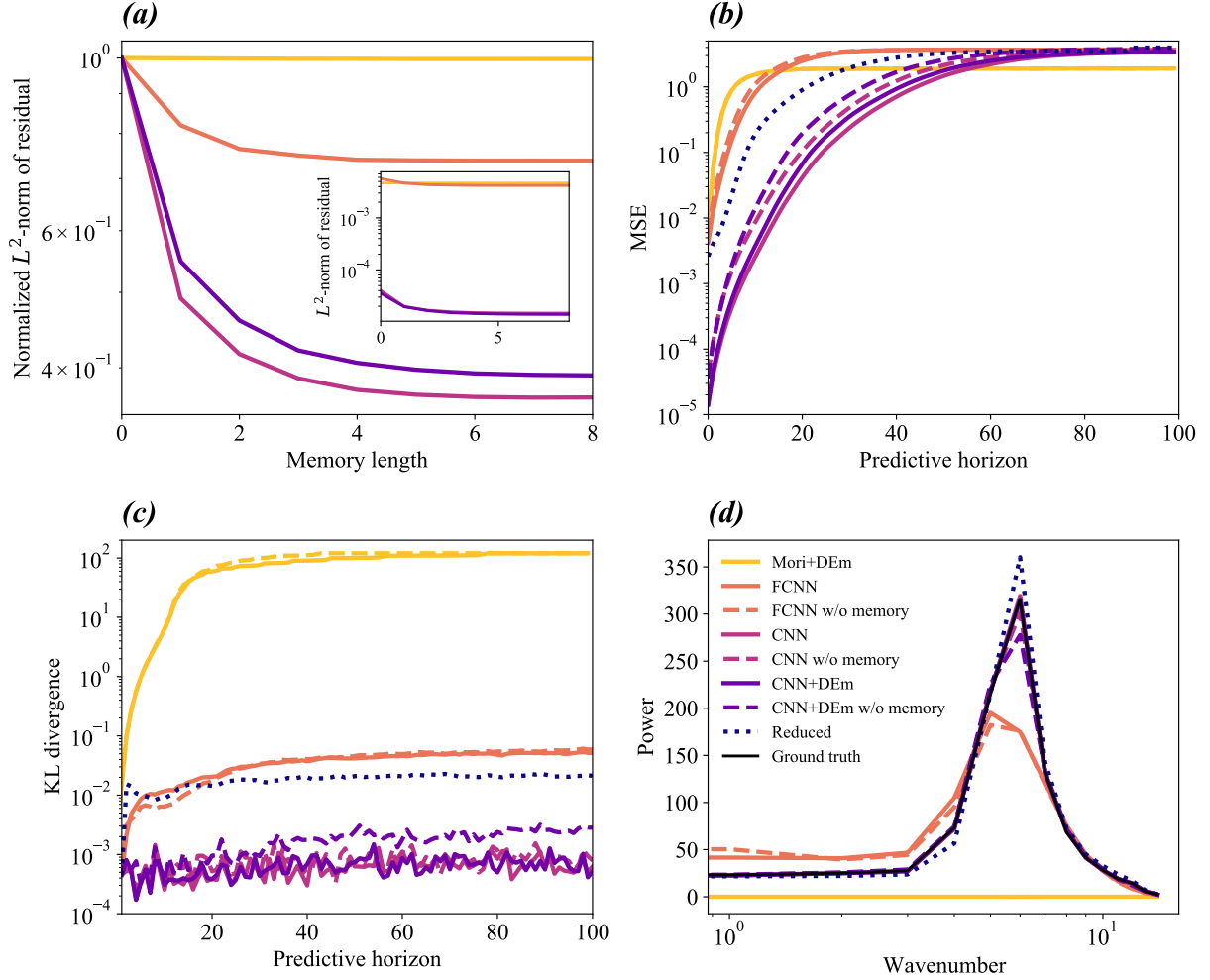


Figure 8: Mori-Zwanzig learning of Kuramoto–Sivashinsky system with regression-based projection operator. (a) The mean squared error of the learned models as a function of memory length. (b) The mean squared prediction error over different prediction horizon. The Lyapunov time for chosen domain size $L = 16\pi$ is approximately 12.56. (c) The Kullback–Leibler divergence of the marginal $(u(t, x_{4i}) \forall i = 0 \dots 31)$ ground-truth distribution from the predicted distribution as a function of prediction horizon. (d) The power spectrum of different models at a prediction horizon 100.

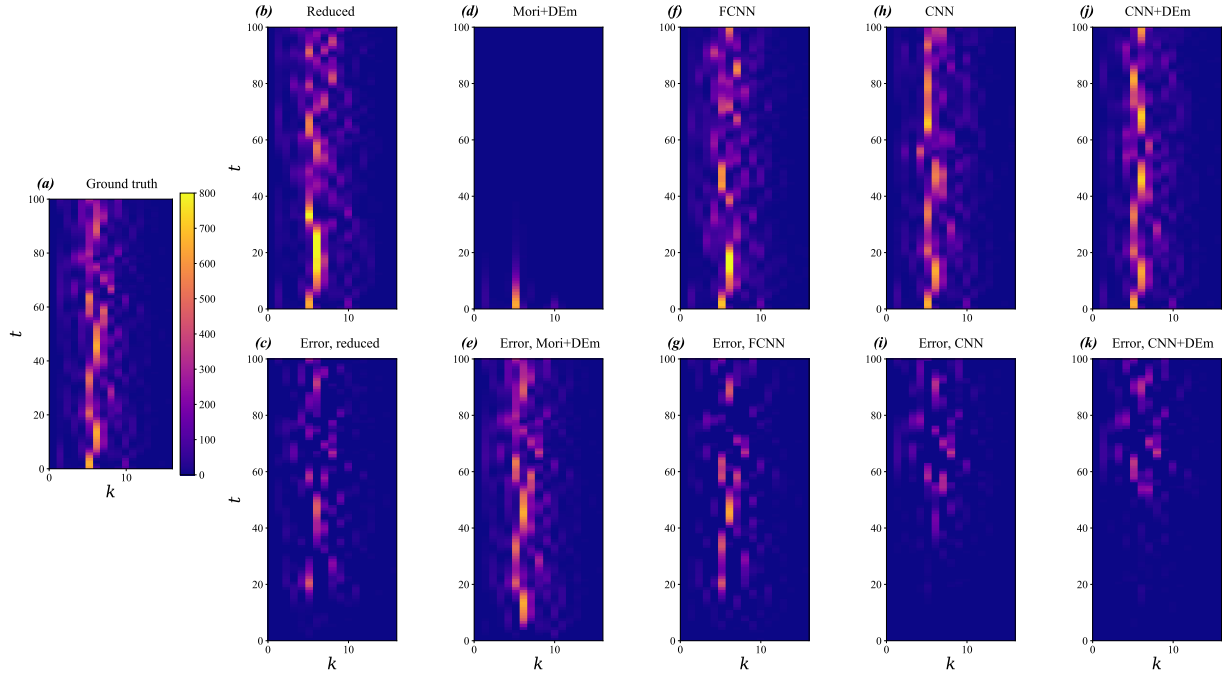


Figure 9: Projection-based Mori–Zwanzig learning of Kuramoto–Sivashinsky system. (a) ”Ground-truth“ spectrum of the coarse-grained trajectory. (b, d, f, h, j) Predicted spectrum using reduced-order simulation and four regression based Mori–Zwanzig models and (c, e, g, i, k) error of the predicted spectrum.

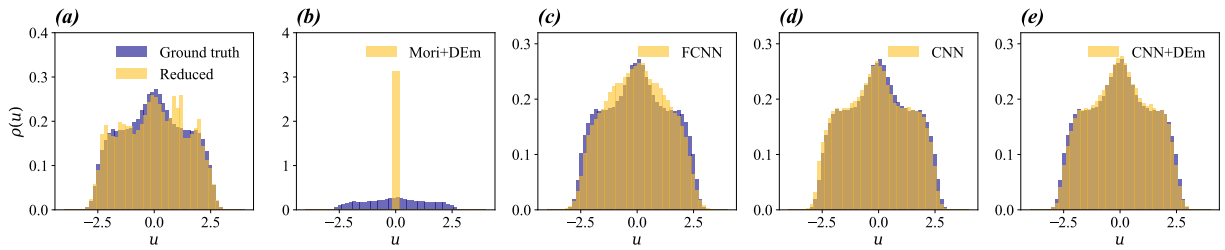


Figure 10: Projection-based Mori-Zwanzig learning of Kuramoto-Sivashinsky system. (a-e) PDFs of long-time predicted trajectories (horizon = 10,000) for five regression-based MZ models.

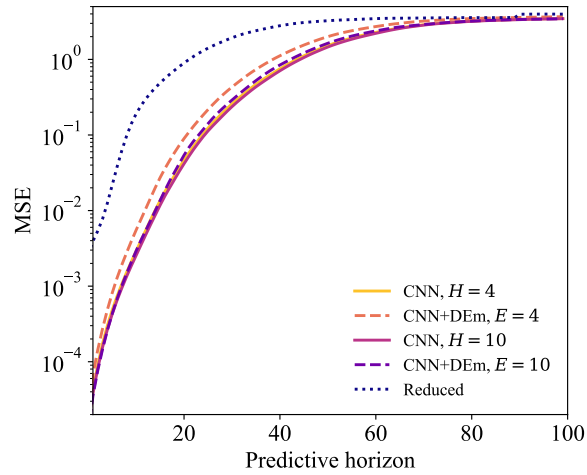


Figure 11: Mori–Zwanzig learning of Kuramoto–Sivashinsky system with various CNN-based regression model. The mean squared error of the prediction as a function of the prediction horizon. The CNN-based MZ models with different MZ memory lengths ($H = 4$ and $H = 10$) are compared with corresponding delay-embedded models with identical set of embedding lengths ($E = 4$ and $E = 10$). The CNN architectures for this numerical experiment are specially designed such that: (1) the total number of parameters of both CNN-based MZ model and CNN-based delay-embedded model are the same and (2) the same information, i.e. the length of the past history, is used for making prediction for both models ($H=E$).